Solid Earth Discuss., https://doi.org/10.5194/se-2018-106
Manuscript under review for journal Solid Earth
Discussion started: 11 October 2018

Solid Earth
Discussions
Open Access
EGU

A new methodology to train fracture network simulation using Multiple Point Statistics

Pierre-Olivier BRUNA[(1)*], Julien STRAUBHAAR[(2)], Rahul PRABHAKARAN[(1, 3)], Giovanni BERTOTTI[(1)], Kevin BISDOM[(4)], Grégoire MARIETHOZ[(5)], Marco MEDA[(6)].

(1) Department of Geoscience and Engineering, Delft University of Technology, Delft, the Netherlands.
(2) Centre d'hydrogéologie et de géothermie (CHYN), Université de Neuchâtel, Emile-Argand 11, CH-2000 Neuchâtel.
(3) Department of Mechanical Engineering, Section of Energy Technology, Eindhoven University of Technology, Eindhoven the Netherlands.
(4) Shell Global Solutions International, Kessler Park 1, 2288 GS Rijswijk, The Netherlands
(5) University of Lausanne, Institute of Earth Surface Dynamics (IDYST) UNIL-Mouline, Geopolis, office 3337, 1015 Lausanne, Switzerland
(6) ENI Spa, Upstream and Technical Services, San Donato Milanese, Italy.

* Corresponding author, p.b.r.bruna@tudelft.nl

Keywords: geostatistics, multiple training images, probability map, fracture networks, stress-induced fracture aperture, outcrop.

Abstract

Natural fractures have a strong impact on flow and storage properties of reservoirs. Their distribution in the subsurface is largely unknown mainly due to their sub-seismic scale and to the scarcity of available data sampling them (borehole). Outcrop can be considered as analogues where natural fracture characteristics can be extracted. However, acquiring fracture data on outcrops may produce a large amount of information that needs to be processed and efficiently interpreted to capture the key parameters defining fracture network geometry. Outcrops thus become a natural laboratory where the interpreted fracture network can be tested mechanically (fracture aperture, distribution of strain/stress) and dynamically (fluid flow simulations (Bisdom et al., 2017).

The goal of this paper is to propose the multiple point statistics (MPS) method as a new tool to quickly predict the geometry of a fracture network in both surface and subsurface conditions. This sequential simulation method is based on the creation of small and synthetic training images representing fracture distribution parameters observe in the field. These training images represent the complexity of the geological object or processes to be simulated and can be simply designed by the user. In this paper we chose to use multiple training images and a probability map to represent the fracture network geometry and its potential variability in a non-stationary manner. The method was tested on a fracture pavement (2D flat surface) acquired using a drone in the Apodi area in Brazil. Fractures were traced manually on images of the outcrop and constitute the reference on which the fracture network simulations will be based. A sensitivity analysis emphasizing the influence of the conditioning data, the simulation parameters and the used training images was conducted on the obtained simulations. Stress-induced fracture aperture calculations were performed on the best realisations and on the original outcrop fracture interpretation to qualitatively evaluate the accuracy of our simulations.

The method proposed here is innovative and adaptable. It can be used on any type of rocks containing natural fractures in any kind of tectonic context. This workflow can also be applied to the subsurface to predict the fracture arrangement and its fluid flow efficiency in water, heat or hydrocarbon reservoirs.

I] Introduction

I.1 The importance of the prediction of fracture network geometry

Fractures are ubiquitous in Nature and are known to impact fluid flow and fluid storage in water (Berkowitz, 2002; Rzonca, 2008), heat (Montanari et al., 2017; Wang et al., 2016) and hydrocarbon reservoirs (Agar and Geiger, 2015; Lamarche et al., 2017). They are typically

Solid Earth Discuss., https://doi.org/10.5194/se-2018-106
Manuscript under review for journal Solid Earth
Discussion started: 11 October 2018

organised as networks ranging from nanometre to multi-kilometre scale (Zhang, 2016), and present systematic geometrical characteristics (i.e. type, orientation, size, chronology, topology) that are inherited from specific stress and strain conditions. These conditions are typically well known in folded (Suppe, 1983, 1985; Tavani et al., 2015; Watkins et al., 2017), faulted (Faulkner et al., 2010; Matonti et al., 2012; Micarelli et al., 2006) and burial-related contexts (Bertotti et al., 2017; Bisdom, 2016) and have been used to derive concepts of fracture arrangements. These concepts are currently used to predict reservoir heterogeneity and to define potential permeability pathways within the rock mass (Lamarche et al., 2017; Laubach et al., 2018). Despite the existence of these concepts, fracture networks generally present an intrinsic complexity (e.g. variability of orientation, local occurrence of new fracture family, change of topology relationships) due, among others, to local variability of the orientation and magnitude of stresses. This makes fractures hard to predict. Moreover, fractures in subsurface reservoirs are largely unknown due to their sub-seismic size and to the scarcity of available data, which is generally limited to borehole information.

I.2 Surface rocks as multiscale reservoir analogues

In this context, the study of outcrop analogues is one of the few ways to constrain the architecture of fracture networks (Bisdom et al., 2014; Bruna et al., 2017; Lamarche et al., 2012; Lavenu, 2013). Outcrops can be considered as a natural laboratory where the structural reality can be observed and quantified at various scales. At the small – measurement station – scale (order of 10's m), fracture type, chronologies and topology relationships can be characterised using classical ground-based structural geology method such as scanlines (Lavenu et al., 2013; Mauldon et al., 2001). At the intermediate – outcrop – scale (order of 10^2's m), length of fractures and geometry variability can be qualified and quantified using unmanned aerial vehicles (UAV - drones). Working on outcrops allows an understanding of

the geological history of the targeted area and eventually to decipher how, when and where fractures were developed. In addition, outcrops constitute an efficient experimental laboratory where some of properties of the fracture network (i.e. fracture distribution, apertures, permeability and fluid flow behaviour) can be known and modelled (Bisdom et al., 2017). At the large – reservoir – scale (order of $10^{3\text{-}4}$m) satellite imagery and geophysical maps provide the characterisation of the 100's of meter long objects such as large fracture systems or faults.

I.3 Modelling approaches classically used to model fracture network geometries

The widely used discrete fracture network (DFN) stochastic modelling tools are providing statistical representation of fracture network constrained generally by univariate and random distribution of orientation, size, spacing and density/intensity data (Bisdom et al., 2014; Bisdom et al., 2017; Huang et al., 2017; Panza et al., 2018). The generated models implicitly follow a local stationarity hypothesis suggesting the invariance of all of the generated statistics by translation in the simulated domain (Deutsch and Journel, 1997; Gringarten and Deutsch, 1999; Gringarten and Deutsch, 2001; Journel and Zhang, 2006). Liu et al., (2009), highlighted the implicit randomisation that conventional discrete fracture networks models produce and demonstrated that parameters like fracture connectivity are poorly considered in these representations. In addition, it is generally admitted that discrete realisations of thousands of fractures objects at the kilometre scale are computationally very demanding and often even impossible (Jung et al., 2013). Some authors attempted to use a pixel-based method to try to predict fracture network geometries. Bruna et al., (2015), used a dense hydrogeological borehole survey sampling a Lower Cretaceous aquifer in the SE of France to define fracture facies and to model their distribution with two-points geostatistics. In this case, the amount of available data and their consistency helped to provide realistic results.

However, far from conditioning data (i.e. boreholes) the fractures simulation are under constrained.

I.4 Multi-point statistics as an alternative to classic DFN approaches

Since Liu et al., (2002), few authors highlighted the potential of using multi-point statistics (MPS) to generate realistic fracture networks (Chugunova et al., 2017; Karimpouli et al., 2017). Strebelle, (2002) showed how the MPS are able to reproduce any type of geological heterogeneities of any shape at any size as long as they present a repetitive character. This characteristic seems particularly well adapted to predict the geometry of a fracture network. The MPS method uses training images (TI) to integrate conceptual geological knowledge into geostatistical simulations (Mariethoz, 2009). The TI is a grid containing geological patterns that are representative of a certain type of geological structure, type and arrangement. The TI can be considered as a synthetic model of the geological heterogeneity (i.e. all the elements characterising a geological object) likely to occur in a larger domain (i.e. reservoir, aquifer, outcrop). The TI must include the possible range and shape of the geobodies that the geoscientist intends to model, as well as the relationship these geobodies have with each other (Mariethoz, 2009; Strebelle, 2002).

I.5 Objectives and contents of this research

In this paper we propose a MPS workflow considering fracture network geometry variability over full outcrops and a methodology on how to use this method at the reservoir scale. The approach is based on the direct sampling method (Mariethoz et al., 2010) and uses multiple training images for a single realisation (Wu et al., 2008). The concept of the probability map has been revised here to define where a training image should be used in the simulation grid. Our outcrop-based simulations also take into account “seismic-scale” objects (i.e. object

longer than 40m) considered as hard conditioning data. The proposed workflow is tested on outcrops considered as analogues of the Potiguar Basin, Brazil where fracture network have been previously characterised and interpreted from drone imagery (Bertotti et al., 2017; Bisdom, 2016). Uncertainties were evaluated by comparing original outcrop interpretation (done manually by a geologist) with the geometrical characteristics of the network generated from MPS. To evaluate the quality of the simulations, we computed mechanical and hydraulic apertures in outcrop fracture interpretation and on the obtained stochastic models. The proposed approach breaks new ground as it provides a quick and efficient way to represent fracture network arrangements at various scales.

II] Methodology

II.1 The direct sampling method

The direct sampling method (DS) was introduced by (Mariethoz et al., 2010). Figure 1, synthesizes the DS modelling process developed thereafter. The method requires a simulation grid where each node is initially unknown and called $\boldsymbol{x}$, a training image grid (TI) where each node is known and called $\boldsymbol{y}$ i.e. V(y) is defined where V is the variable of interest (e.g. facies value). The simulation proceeds as follows. First, the set of conditioning data (if present) is integrated in the simulation grid. Then, each remaining unknown node $\boldsymbol{x}$ is visited following a random or defined path, and simulated as follows. 1) The pattern $\boldsymbol{d_n(x)} = \boldsymbol{(x_1,V(x_1)),\ldots,(x_n,V(x_n))}$ formed by the at most $\mathbf{n}$ informed nodes the closest to $\boldsymbol{x}$ is retrieved. Any neighbour $\boldsymbol{x_i}$ of $\boldsymbol{x}$ is either a previously simulated node or comes from the conditioning data set. The lag vectors $\boldsymbol{h_i} = \boldsymbol{x_i}\text{-}\boldsymbol{x}$ define the geometry of the neighbourhood of $\boldsymbol{x}$. The combination of the value and position of $\boldsymbol{x}_i$ defines the data event or pattern $\boldsymbol{d_n(x)}$. 2) Then, the TI is randomly scanned to search for a pattern $\mathbf{d_n(y)}$ similar to $\mathbf{d_n(x)}$. For each scan node $\boldsymbol{y}$, the pattern $\boldsymbol{d_n(y) = (y_1,V(y_1)),\ldots,(y_n,V(y_n))}$, where $\boldsymbol{y_i=y+h_i}$, is compared to $\mathbf{d_n(x)}$ using a distance

(Meerschman et al., 2013). When the distance is lower than an acceptance threshold (***t***) defined by the user or if the proportion of scanned nodes in the TI reaches a maximal fraction (f) defined by the user, the scan is stopped and the value of the best candidate ***y*** (pattern with the minimal distance) is directly attributed to ***x*** in the simulation grid (i.e. ***V(x) = V(y)***).

As the DS method does not use a catalogue of all possible patterns found in the TI, it is extremely flexible and in particular allows taking into account both categorical and continuous variables and managing multivariate cases, provided that the pattern distance is suitable. In this paper we are using the DeeSse version of the direct sampling code.

II.2 Multiscale fracture attributes

To evaluate how the direct sampling method is dealing with the fracture network, the present experimentation is based on outcrop data (reference) where the present-day "structural reality" is observable at various scales. Pavements (i.e. horizontal surfaces in the order of 10^2 m scale) were targeted because these objects contain important information that is not always accessible with standard vertical outcrops (Corradetti et al., 2017a; Corradetti et al., 2017b; Tavani et al., 2016) or with classic geophysical imagery. Pavement sizes allow the user to interpret and localise fracture patterns variability (Bruna et al., 2018). For instance, clusters of fractures (i.e. local increase of the fracture density) can be identified by the interpreter. Pavements also allow obtain quantitative data on fracture lengths, which are usually difficult to obtain in vertical cliff objects. In the subsurface, data can be provided by geophysical 3D maps and fracture attribute detection tools (Chopra and Marfurt, 2007; Somasundaram et al., 2017). However, these tools are not always available and detect the longer lineaments only (e.g. > 50 m long depending on the resolution of the imagery).

Working with pavements constitutes an asset as small-scale investigation can be conducted in key zones of the outcrop (i.e. in folded areas, each compartment or dip domain of the fold

should be imaged and investigated in detail) where the gathered data will help to calibrate larger scale information. Classical fieldwork methods (observation and characterisation, measurements, statistical analyses, sampling) help interpreting fracture families and are essential to constrain larger scale observation.

In this study, UAV-based photogrammetry is used to obtain an orthorectified mosaic and 3D digital outcrops models (Bemis et al., 2014; Claes et al., 2017; Vollgger and Cruden, 2016). The scale of these images is an intermediate between the scale of measurement station and that of satellite imagery. Digitization of fracture traces, geological contacts, sedimentary structures and structural domain boundaries are currently processed by hand and represent a considerable time investment. In this contribution, fractures were interpreted in orthomosaic images with the help of GIS software. Length, azimuth, fracture family proportions and fracture density statistics were extracted from the interpretation. In addition, a series of measurement station (area of about 2 × 2 m) information was acquired and compared with the dataset from the drone imagery in order to align interpretations and provide coherent fracture history.

II.3 Training images, conditioning data and probability maps

- **Training images**

Training images (TI) are the base input data of the MPS simulation. Building them is a critical step to succeed a realisation (Liu et al., 2009). The TI is a pixelated image based on a local interpretation of a geological phenomenon (i.e. an interpreted photography taken from a local zone of interest in the field) or digitised by a geologist and based on geological concepts (Strebelle, 2002). These images should synthesise all of the recognized geological parameters that characterise the area to simulate. This implicitly means that the proportion of facies carried by the TI, will be reproduced into the simulation grid but this also requires extensive

pre-processing work. To manage this complexity, we propose to use multiple training images where facies proportion and geometrical distribution can vary. Hence, each TI has a local impact on the simulation. Moreover, in our approach fractures sets are grouped in facies in the TI, based primarily on their orientation and possibly on their length or additional parameters defined by the user. The fractures classification helps reproducing patterns and simplifies the process of building the TI.

- **Conditioning data**

One limitation of the MPS methods is the tendency to disconnect long continuous objects (i.e. typically fractures, (Bruna et al., 2017). To manage this issue, longer fractures can be identified and incorporated into the simulation as conditioning data. As per the training images, these data can be integrated as pixelated grids. They may come from satellite imagery or they can be interpreted from gravity or magnetic surveys or from 3D seismic imagery (Magistroni et al., 2014).

- **Probability map**

The direct sampling method can be used with multiple training images. In this situation, the user provides a set of TIs, and for each TI a probability map defined on the simulation grid, giving at each node the probability to use that TI. The pixel-wise sum of these maps should then be equal to one in every node. If each TI corresponds to a partition of the area of interest, with for each TI one elementary zone, covering the whole simulation grid, the probabilities in the map are set to one for specific TI and to zero for the other ones.

The probability map comes from a simple sketch (i.e. a pixelated image) given by the MPS user. It is based on geological concepts that define the geometry variability over the simulated area. In each of these areas the simulated property will follow the intrinsic stationary hypothesis (Gringarten and Deutsch, 2001; Journel and Zhang, 2006; Journel, 2005) but the entire domain will be non-stationary. These maps provide a large-scale framework that may

be refined and modified with additional data such as measurement stations or drone surveys coming from surface exploration or wells data containing fracture network information.

II.4 Testing the simulated network: from pixels to segments

MPS realisations are produced as pixelated images. To evaluate the resulting fracture network, pixels alignments corresponding to fractures are extracted as discrete straight-line objects defined by starting and an ending x, y coordinates using a custom MATLAB routine. Fractures are separated from the background and in different sets by automatic image classification methods. On grayscale images, this is obtained by multilevel image thresholding through the Otsu's method (Otsu, 1979). On color images, fracture sets are classified based on their color components with the k-means clustering algorithm built in in MATLAB (Lloyd, 1982), on images previously converted to the perceptually uniform Lab color space. Image classification gives in output a series of binary images, one for each fracture set, where lineaments are represented as foreground. The foreground segments are finally fitted with straight lines using the *lineseg.m* algorithm by (Kovesi, 2000), which gives in output a list of starting and ending point coordinates for each fracture set.

III] Results: test case on analogues of the Potiguar Basin, E Brazil

III.1 Geological setting

The Potiguar Basin is a rift basin located in the easternmost part of the Equatorial Atlantic continental margin, NE Brazil (fig. 2). The basin is found both onshore and offshore (fig. 2). The basin was generated after the initiation of the South American and African breakup during the Jurassic - Early Cretaceous times. It was structured by a first NW-SE extension stage latterly rotating to an E-W extensional direction (Costa de Melo et al., 2016). The rift basin displays an architecture of horsts and grabens striking NE-SW and bounded towards the

255 east and south by major faults systems (de Brito Neves et al., 1984), fig. 2). The Potiguar
256 Basin displays three sedimentary sequences deposited since the early Cretaceous times (i.e.
257 syn- and post rift depositions). The last post-rift sequence was deposited from the Albian and
258 encompasses the Cenomanian-Turonian Jandaíra Formation. This formation consists of up to
259 700 m thick bioclastic calcarenites and calcilutites deposited in transgressive shallow marine
260 environment. The stress field affecting the Jandaíra Formation during the Campanian to the
261 Miocene compression was oriented N-S (Bertotti et al., 2017). From the Miocene to the
262 Quaternary the onshore part of the Potiguar basin was uplifted. Synchronously, a new stress
263 field was established trending to a NW-SE direction (Reis et al., 2013).
264
265 **III.2 Outcrop data**
266 The area of interest measures 2.1 × 1.3 km and is located about 25 km NE of the city of Apodi
267 in the Rio Grande Do Norte state (fig. 2). It contains two outcrops AP3 and AP4 (Bertotti et
268 al., 2017; Bisdom, 2016), fig. 2) here defined respectively as 600 × 300 m and 400 × 500 m
269 large pavements localized in the Jandaíra Formation. AP3 and AP4 crop out as pavements
270 with no significant incision. The outcrops are sparsely covered by vegetation and
271 consequently they present a clear fracture network highlighted by karstification. In 2013,
272 images of AP3 and AP4 were acquired using a drone (Bisdom, 2016) and processed using the
273 photogrammetry method. Two high-resolution ortho-rectified images of these pavements
274 (centimetre-scale resolution) were used to complete fracture network interpretation and to
275 extract fracture parameters. In AP3, 775 lineaments were traced (fig. 3) and in AP4, 2593 (fig.
276 4). These lineaments are grouped in this article over the general term “fractures”. For each of
277 these outcrops three fractures sets were identified: set1 striking N135-N165, set2 striking
278 N000-N010/N170-N180 and set 3 striking N075-N105. Fractures falling outside of these
279 ranges were not considered in the input data. Consequently, in AP3 we considered 562 only

(out of 775 fractures traced in the pavement) and in AP4 we considered 1810 only out of 2594 fractures. In addition, ground-based fieldwork was conducted in AP3 and AP4 to understand the structural history of the area and to calibrate the interpretation conducted on the drone aerial photography (Van Eijk, 2014). General location and fracture data are presented in figure 3 and 4 and in table 1.

In AP3, sets 1 and 2 are evenly distributed over the pavement. However, they present intrinsic intensity variability in the area of interest. Set 3 is mainly expressed in distinct regions of the outcrop. Small-scale investigations (conducted on measurement stations in the outcrop) allowed associating set 3 with stylolite and sets 1 and 2 to veins. In addition, sets 1 and 2 present evidences of shear movements and are then considered as a conjugate system.

In AP4 small-scale investigations highlight the same characteristics as the ones observed in AP3. Although the conjugate system (set 1 and set 2) is less developed there than in AP3. It is also notable that more crosscutting relationships were observed in AP4 compared to AP3.

III.3 Input data for MPS simulation

AP3 illustrates the effect of conditioning data and of simulation parameters in the stochastic realisations. To evaluate the effect of conditioning data, results of two simulations were compared, with and without conditioning data. The sensitivity of simulation parameters was investigated by varying i) the number of neighbours defining patterns (data events $\boldsymbol{d_n}$), ii) the acceptance threshold ($\boldsymbol{t}$) defining the tolerance the algorithm authorises to find a matching data event in the simulation grid (Mariethoz et al., 2010) and iii) the fraction of the TI to be scanned during the simulation process to search for data events. Results of this sensitivity analysis help to propose the best possible simulation for AP3 and to optimise the choice of input parameters for AP4 fracture simulation.

AP3 presents intrinsic fracture network geometry variability. This observation emphasizes that averaging fracture parameters on the entire domain is not well suited to represent the complexity of the network. We observed that the length of fracture per sets and the density of fractures are parameters that vary the most here. The analysis of these variations allow to partition AP3 and AP4 in elementary zones and to synthesize the fracture network characteristics in each of these domains. The following section defines how the TI, PM and conditioning data were built.

- **Partitioning, training images and probability map for AP3 and AP4**

We divided AP3 in 5 elementary zones (EZ) based on visual inspection the pavement (fig. 5A-B). The number of fractures per EZ is synthesized in the figure 5. The proportion of fracture per elementary zone is available in table 1. A limited part of the fractures belong to two neighbours elementary zones. This issue is quantified in table 1.

A probability map with sharp boundaries (fig. 5B) was created for AP3. Sharp boundaries are justified by the variability of the network geometry, which is known from the visual inspection of the interpreted image. Smooth transitions could also be defined (see discussion). The input data to build the probability map is an image of the partition of the area of interest containing the different outcrops. In this image, the indexed zones (elementary zones EZ) are characterised by a distinctive colour.

The goal of this research is to show that MPS is able to accurately reproduce an existing fracture network (interpreted on AP3 outcrop) from small and simplified sketches (training images) representing what the network should look like in each elementary zone. At the scale of a reservoir where some outcrops analogues and fracture tracing may be available, the "interpreted reality" of the network can be directly used as a training image. We chose to ignore the tracing and to rely on parameters that are classically available without having access to drone images of an entire outcrop (i.e. orientation, spacing, abutment) and to

compare the interpretation with the simulated network. In that respect fracture orientation were averaged to a single value. Hence, set 1 strikes N150, set 2 strikes N000 and set 3 strikes N090. According to the outcrop partitioning, five training images were created (fig. 5C). In each training image, three facies corresponding to the three fracture sets were created. Set1 (N090) is green, set 2 (N150) is red and set 3 (N000) is blue (fig. 5C). Topology is a crucial problem in fracture simulations because it influences the connectivity of the network. In the MPS simulations abutments are particularly well reproduced as they represent singular pixels arrangements that are efficiently taken into account. However, crosscutting relationships imply the use of a different facies at the intersection locus. This method respects and reproduces intersections during the simulation process. In AP3, the analysis of the topology relationships showed three main crosscutting interactions:

- Long N150 cross-cut long N000 fractures (conjugated sets)
- N000 cross-cut N090
- N150 cross-cut N090

To take into account these topological parameters a different facies colour was attributed to the cross-cutting locus (the crossing facies, fig. 6). When the MPS realization will be later discretized, the younger fractures will be truly represented as continuous segments. The older fractures will be cut in pieces but their alignment will be, in most of the case, maintained during the simulation process.

- **Dimensions of the simulations grids and of the training images**

The dimensions of the simulation grid for AP3 and of each training image (in pixels) are shown in fig.5. The number of pixels is automatically determined by the size of the original drawing made by the geologist.

The size of the input training image is generally not influencing the simulation. However, it has to be chosen sufficiently large with respect to the complexity of the patterns in order to

Solid Earth Discuss., https://doi.org/10.5194/se-2018-106
Manuscript under review for journal Solid Earth
Discussion started: 11 October 2018

354 get reliable spatial statistics. The DS method tends to identify patterns (i.e. $\boldsymbol{d_n}$'s see above) in
355 the TI and to paste them into the simulation grid. However, at a constant resolution and
356 specifically for fractures patterns, it is likely that a 50 × 50 m training image will carry more
357 complexity and variability than a 10 × 10 m one. This parameter should be taken into
358 consideration when starting digitizing training images, especially when spacing between
359 fractures is not consistent across the simulation grid.

360 • **Long fractures conditioning**

361 Because the MPS method has the tendency to cut long individual segments into smaller
362 pieces, the fractures longer than 40 meters – the ones visible from satellite/drone imagery in
363 AP3 – where isolated and considered as hard conditioning data (fig. 5D). This threshold was
364 arbitrarily determined from the dataset we have. In AP3, less than 8% of the fractures are
365 longer than 40 m.

366 In AP3, long fractures belong only to the sets oriented/striking N000 or N150 (fig. 5D). 18
367 N000 fractures (3% of the whole) and 30 N150 fractures (5% of the whole) were digitized and
368 integrated as conditioning data in the simulation.

369

370 **III.4 Outcrop scale simulations**

371 **III.4.1 Impact of conditioning data on AP3 simulations**

372 In AP3, the 50 long fractures were manually digitized and imported into the simulation grid as
373 categorical properties to be considered as hard conditioning data during the MPS simulation
374 process. The MPS simulation is consequently in charge of stochastically populating the
375 smaller factures within the grid.

376 Results of the influence of these data are presented in figure 7. The principal simulation
377 parameters in the considered scenarios (with and without conditioning data) were set up

Solid Earth Discuss., https://doi.org/10.5194/se-2018-106
Manuscript under review for journal Solid Earth
Discussion started: 11 October 2018

identical (constant acceptance threshold (5%), constant percentage of scanned TI (25%) and constant number of neighbours (50)).

Results showed that the realisation without conditioning data creates 20% less fracture than the original outcrop reference. The simulation with conditioning data creates 9% less fractures than AP3, which makes the simulation satisfactory. It is also remarkable that the non-constrained simulation represents only 23 fractures above 40 meters (compared to the 50 long fractures interpreted on the AP3 outcrop). In this simulation the long fractures are essentially located in the zone 3 of the outcrop. Because the simulation is a stochastic process, the location of the long fractures is randomly determined in the absence of hard conditioning data. Considering hard-conditioning data also gives a more realistic representation of the fracture network.

III.4.2 Sensitivity analysis on the AP3 simulation parameters

- **Simulation parameter set-ups, duration and analyses conducted on the results**

Simulation parameters were varied for each simulation in order to emphasize their effect on each realisation. One realisation per test was performed during this analysis. The goal of this analysis is to show how the different parameters influence the reproduction of fracture segments and not to evaluate how good is the matching between the simulation and the reference.

The MPS realisations are pixelated images. The sensitivity analysis is based on the discrete segments extracted from these pixelated images (see II.4). All of the simulations present a variable percentage of segment lengths that are below the minimal fracture length interpreted in the AP3 outcrop (i.e. simulation noise). Consequently all segments smaller than 2.2m where removed from the simulation results. A length frequency distribution was compiled for each of the generated simulations.

403 The influence of the number of neighbours was evaluated trough 7 simulations (SIM1 to
404 SIM7). The acceptance threshold and the number of neighbours was investigated by
405 comparing 8 simulations (SIM8 to SIM15) where the scanned fraction of the TI was fixed at
406 25%. The percentage of the scanned fraction of the TI was combined with the 2 other
407 simulation parameters. This combination was tested over 12 simulations (SIM16 to SIM27).
408 The models set-ups and the duration of the simulations are presented in (table 2). Tt is notable
409 that SIM8 / SIM9, SIM10 / SIM11 and SIM13 / SIM14 produce exactly the same network
410 despite the modification of the simulation parameters. Also The MPS algorithm successfully
411 performed SIM16 but the segment extraction generated an error preventing the discretisation
412 of all of the objects. No solution was found to solve this issue.
413 The total amount of generated fractures was counted and compared with the total number of
414 fractures interpreted from the original outcrop. A deviation of 10% compared to the original
415 amount of interpreted fractures is considered as a satisfactory result as it is very close to the
416 reference amount of fractures. A deviation of 20% compared to the original amount of
417 interpreted fractures is considered as an acceptable result. This deviation is consequent but
418 can be adjusted by varying the simulation parameters. A deviation above 20% was rejected as
419 a complete reconsideration of the parameters is required. Results are synthesized in table 3.
420 The total amount of segments was initially counted in the entire simulation domain. The sum
421 of segment per part is constantly higher than the initial total amount of segments because
422 segments cutting a sharp boundary are divided in two - segments falling within two
423 elementary zones and are consequently counted twice. The number of generated fractures per
424 simulation zone was also computed and the same deviation thresholds were applied to
425 evaluate if the simulation is satisfactory, acceptable or rejected. Tables 4 to 6 synthesize the
426 sensitivity analysis conducted of 27 realisations of the AP3 outcrop.

427 The length of the segments have been computed for each realisation and are presented in
428 figure 8.
429 The influence of the hard conditioning data and of the drawing of the training image was also
430 quantitatively investigated and compared respectively with the length of the generated
431 segments and with the amount of segments generated per zones
432 • **Summary of the results**
433 Increasing the number of neighbours rises the computation time (table 2, SIM 1 to 7). A small
434 amount of neighbours results in a noisy simulation (table 2, SIM1). The contrary lead to a
435 downsampling of the generated segments that becomes longer than the interpreted fractures in
436 AP3 (table 2, SIM7). Decreasing the acceptance threshold leads to an increase of the
437 simulation time (table 2 SIM8-15). Increasing the scanned fraction of the TI is the most time
438 consuming operation (table 2 SIM17-27).
439 Increasing the number of neighbours only is generally not sufficient to accurately generate a
440 satisfactory or acceptable total amount of fractures (table 3). Increasing the scanned fraction
441 of the TI produces in all cases the closest total number of fractures compared to the reference
442 outcrop (table 3).
443 The counting of fractures in simulation zones revealed that set 2 and set 3 in zone 1, set 3 in
444 zone 4 and set 1 in zone 5 are generally underestimated during the simulation process. In
445 contrast, fracture set 1 in zone 2 is generally overestimated. The consistency of the error over
446 almost the entire set of simulations indicates an issue on the training image representation
447 (table 4-6). Increasing the scanned fraction of the TI generally allows to better represent a low
448 proportion of fracture facies within a TI (Zone TI5, set 2, table 6).
449 An acceptance threshold below 5% leads to an overestimation of the number of small
450 fractures (between 0-10 m), fig 8. In this case, amount of segments between 0-20 m is
451 generally close to the reality. Increasing the scanned fraction of the TI produces the highest

Solid Earth Discuss., https://doi.org/10.5194/se-2018-106
Manuscript under review for journal Solid Earth
Discussion started: 11 October 2018

quantity of fractures ranging from 0-10 m (fig. 8). Increasing the number of neighbours and the percentage of the scanned TI will result in an increase of the length of the fractures used as hard conditioning data. However, the fracture elongation does not affect all of the hard conditioned fractures and represents a very small percentage of the whole modelled fracture network.

III.4.3 Attempt at an optimisation: OPT1

OPT1 was parameterised in regard of the previous observations in order to generate a simulation that is the closest-to-reality possible. For this purpose, the amount of fractures from set 2 and set 3 drawn in TI1 and set 3 drawn in TI4 was increased. In contrast, the amount of fractures from set 1 drawn in TI2 was decreased significantly (fig. 9). We choose to setup the number of neighbours at 50 and the acceptance threshold at 2%. TI1 and TI4 will be scanned at 75% and the rest of the TIs will be scanned at 50% (table 2).

The simulation time for the proposed simulation is 2 min 31s (table 2). The total amount of generated fractures is satisfactory compared to the amount of fractures interpreted in the original outcrop.

To evaluate the repeatability of the optimised simulation, 6 realisations using the same parametrisation were generated for OPT1. The total amount of fracture generated for these simulation always fall below the 10% deviation compared to the reference outcrop.

The number of segments comprised between 0-20 m in OPT1 is slightly above the satisfactory deviation limit. As per all the generated simulations, the number of fractures between 2.21 m and 10 m is largely overestimated.

OPT1 contains a more satisfactory and acceptable fracture count than any other simulation generated before (table 6). The amount of segments generated in zone 1 and 2 for set 1slightly overestimate the amount of segments. In zone 3, OPT1 fails to represent the amount of

Solid Earth Discuss., https://doi.org/10.5194/se-2018-106
Manuscript under review for journal Solid Earth
Discussion started: 11 October 2018

fractures for set 1 (25% deviation) and for set 3. Fracture set1 in zone 4 is largely overestimated.

III.4.4 Using the sensitivity analysis results to model AP4

As per AP3, AP4 present intrinsic fracture network geometry variability. This outcrop was divided in 3 elementary zones (fig. 10A-B). According to AP4 partitioning, a probability map with sharp boundaries (fig. 10B) was created. For AP4, the configuration of the outcrop led to mask the area where no interpretation data were performed. In these particular zones a "no data value" was attributed and these masked areas were excluded during the modelling process. In AP4 three training images were created (fig. 10C). As per AP3, the size of the AP4 simulation grid was doubled compared to its original dimension (available in fig.10). In AP4, fractures longer than 40 meters were also considered as hard conditioning data. Here, less than 1.5% of the fractures are longer than 40m (fig. 10D). In AP4, long fractures were found in the 3 sets and mainly in the south-eastern part of the outcrop (fig. 10D, elementary zone 6). 11 N000 fractures (0.5% of the whole), 13 N150 fractures (0.6% of the whole) and 9 N090 fractures (0.4% of the whole) were digitized and integrated as conditioning data into the simulation.

Based on the results of the sensitivity analysis of AP3 we generated one simulation for the AP4 outcrop (fig. 11). The modelling parameters for SIM AP4-1 were selected as following: the number of neighbours was set up at 50 and the acceptance threshold at 2%. The 3 training images used in the simulation are presented in figure 11 and are considered as representative of the fracture arrangement in each region of simulation. The scanning percentage of TI6 and TI7 was set up at 50%. The scanning percentage of TI8 was set up at 100% because a lot of small segments need to be represented. With this configuration, the simulation lasts slightly more than 5 minutes. The fact of intensely scanning TI8 is probably responsible of this

duration. Analysis was conducted on the total amount of segments generated and of segments per set of fractures. In AP4 the total number of segments is 1810. The simulation realises 1682 segments in total, which constitutes a satisfactory result. AP4 original presents 252 segments striking N150 (set 1), 856 segments striking N000 (set 2) and 702 segments striking N090 (set 3). The results of Simulation AP4-1 are always satisfactory or acceptable with 206 segments striking N150 (set 1), 834 segments striking N000 (set 2) and 642 segments striking N090 (set 3). A detailed analysis was not conducted here because AP4 contains a lot of small fracture intersections (especially in the TI8 zone) and this makes the segment extraction a complex process. However, these results are promising for the future.

IV] Uncertainty analysis

IV.1 Smooth transitions between elementary zones: towards reservoir scale models

The strength of the method proposed here relies on the use of a probability maps and on the opportunity to consider multiple training images in a single realisation to generate non-stationary models of fracture network geometries. In the case of AP3 and AP4, the probability maps are essentially constrained by the variation of geometry of the fracture networks observed on the geological interpretation made on the drone imagery. Consequently, the defined areas are pragmatically bounded and the nature of the limit between one zone and another is a sharp boundary.

AP3 and AP4 outcrops are separated by about 2.5 km and very little is known about the fracture network geometry between these two locations. Assuming that there is no major structural deformation (fold or faults) that may cause a change in fracture geometry at the close vicinity of the outcrop “reality”, zones initially defined on the AP3 and AP4 outcrop can be extended to the limits of the reservoir-scale model boundaries (fig. 12). In this particular

case, filling the gap between the two outcrops appears to define how the transition between one side of the simulation grid and the other should be determined.

Fractures are localised objects that do not need to be necessarily continuous from one simulation zone to another. The constant higher proportion of the non-fractured matrix facies versus localised and thin fracture elements ensures the coherency and relative compatibility from one simulation region to another. The idea of the simulation grid region partitioning was re-evaluated and an alternative method, using probability of inverse distance proportion, was proposed here. Contrarily to the definition of sharp boundaries in the probability maps used for AP3 and AP4, as probability map with smooth transitions is defined as if each TI correspond to a partition of the area of interest, with for each TI one elementary zone, covering a part of simulation grid, the probabilities in the map are set to one for specific TI and to zero for the other ones. On each remaining zones, called transition zones, one has to define which TIs may be involved. On a transition zone, the probabilities of involved TI's are set proportional to the inverse distance to the elementary zones of the corresponding TI's. This process creates smooth transitions in low constrained area decreasing the influence of one TI towards another (from one elementary zone to another).

No faults or folds can be initially identified between AP3 and AP4 to condition the drawing of the probability map. In this first case, a rectangular compartment representing a gradual probability transition to use the training image associated to one outcrop or to the other filled the blank space between the two outcrops. For instance, fig 12E shows in the Transition_Zone_1 a decreasing probability to use TI1 from left to right (i.e. zone 1 to zone 6) and conversely to use TI6 from right to left.

Recently, investigations conducted on the Rio Grande do Norte geological map (Angelim et al., 2006), demonstrated the presence of a fault crossing the simulation grid near the AP3 zone. This structure may explain the variability of fracture geometry from AP3 (EW stylolites

552 and strong presence of conjugated NS/NW-SE system) to AP4 (EW stylolites associated to
553 NS fracture) system, the NW-SE conjugated system is here subordinate). Further geological
554 investigations need to be conducted in this particular place to proof the influence of this fault
555 on the network geometry. However, fig 12F, shows an alternative probability map taking into
556 account this interpretation and present how flexible the probability map can be. The proposed
557 method demonstrates its adaptability in various geological contexts.
558
559 **IV.2 Evaluation of the accuracy of the simulation using mechanical**
560 **modelling**
561 Uncertainty analysis is required while performing simulations of geological parameters,
562 especially far from input data. The sensitivity analysis presented in this paper is a way to
563 appreciate how good the result provided by the MPS simulation is compared to the reference.
564 However, this test has little meaning when the reference is unknown (e.g. subsurface).
565 In this case the evaluation of fracture network permeability (i.e. which of the considered
566 fractures are open and are potentially capable to conduct fluid from one point to another) can
567 be tested dynamically and appears to be a good way to validate the provided simulation. This
568 approach can also be extended to fluid flow simulations through the permeable fractures. We
569 calculated mechanical and hydraulic apertures using a Barton-Bandis stress induced aperture
570 model (Barton, 1982; Barton and Bandis, 1980) on the original AP3 interpreted outcrop and
571 on four selected MPS realisations.
572 Flow in naturally fractured reservoirs is driven by the occurrence of open fractures. The
573 contribution of fractures to fluid flow at in-situ stress conditions in reservoir models can be
574 defined by the Mohr-Coulomb critical stress method (Hoek and Martin, 2014; Rogers, 2003).
575 If shear stress acting on a fracture exceeds normal stress it becomes critically stressed and
576 forms a conduit to flow. The fracture aperture is a key parameters to know for reservoir

577 evaluation and production. The Barton-Bandis empirical model quantifies the aperture that
578 remains when irregular mismatching fracture walls are partially closed under in-situ stress
579 (Fig. 13). The theory and equations behind the use of the Barton-Bandis model are presented
580 in the appendix A of this article.
581 We chose four MPS generated simulations and the original interpreted fracture dataset for the
582 aperture calculations. We used ABAQUS (Dassault Systemes), a commercial finite element
583 solver for the stress calculations. A conformal mesh consisting of triangular elements is
584 generated around the fracture traces, which are represented as lower dimensional polyline
585 seams within a 2D plane strain geometry. The number of elements used to mesh the
586 geometries in AP3 original interpreted outcrop is 282020, in SIM1 is 277172, in SIM7 is
587 272598, in SIM26 is 277778 and in OPT1 is 276702.
588 An anisotropic load is applied on the four edges of the model to replicate a scenario where the
589 maximum horizontal stress is thrice the minimum horizontal stress in the displacement-
590 loading step. The normal local stress and shear slip, which is heterogeneous, and variable
591 across fracture trace length is hence calculated for the entire fracture system. Longer fractures
592 and intersecting fractures have a larger tendency to slip. Also fractures, which are
593 preferentially aligned to the maximum horizontal stress, would have a greater magnitude of
594 local normal stress. The parameters used for the simulations are tabulated below:

595

$Sh_{max} = 30MPa$	$\nu = 0.3\ (-)$	$JRC = 15\ (-)$
$Sh_{min} = 10MPa$	$E = 35\ GPa$	$JCS = 120MPa$

596 The resulting aperture distributions can be seen in figure 14. A qualitative comparison of the 5
597 different DFN's hydraulic aperture distributions demonstrated similar heterogeneities. There
598 are areas within the network, which are open to flow, but also regions, which serve as flow
599 bottlenecks and hence would have a lower permeability. The actual effective permeability of
600 the fractured system under stress would however depend upon the balance between the matrix

permeability versus the heterogeneous fracture permeability. Our results indicate that the MPS generated fracture realizations preserve similar regions of open and closed apertures when compared with the deterministic outcrop derived network.

V] A method to create 3D DFN out of 2D MPS realisations

The MPS simulation outputs presented in this paper are on the form of 2D pixelated maps. MATLAB codes were developed to extract starting and end point coordinates (georeferenced) of a series of aligned colorized pixels that represent a fracture trace from these images. Transforming this output in geologically realistic 3D surfaces is not easy. (Karimpouli et al., 2017) studied samples coming from coalbed methane reservoirs in the fractured Late Permian Bowen Basin in Australia. They realised multiple 2D and pseudo 3D images (i.e. orthogonal 2D images) and used the cross-correlation based simulation (CCSIM) to represent the internal organisation of coal cleats and the heterogeneity of the coal matrix in 3D. Their approach greatly improved the understanding of the internal complexity of coal samples and gives better results than classical DFN's based on averaged distributions. However, their method requires an important initial amount of information (i.e. CT scans slices used as training images) that is generally not available at a larger scale. The use of MPS in 3D seems particularly not suited for fracture network representation because: i) they require to associate fractures from 2D map view and from 2D section view (3D or pseudo-3D), ii) it appears difficult to consider isolated fractures in this type of approach and iii) in the subsurface fracture height and/or fracture length are generally unknown.

To tackle these problems, we choose to generate statistic fracture networks in 2D map environment only. In the presented approach, the 3D is obtained by extruding 3D fracture planes in fracture units (fig. 15). In this approach we consider that fractures are entirely bound to the units, which can appear as a limitation if isolated or aborted fractures occurs inside a

layer. However, we can consider variable levels of fracture units. Figure 15 presents an hypothetic scenario where red fractures are confined to a large fracture unit (FU1) cross-cutting smaller ones (FU4 containing also smaller red fractures but smaller. In such a representation, one 2D planar simulation is required at each top mechanical unit to generate a new set of fracture.

In real-world subsurface configurations, mechanical units can be extracted from well logs (resistivity, density, lithology; Laubach et al., 2009). In outcrop, the resort to vertical cliffs adjacent to 2D horizontal pavement is required to define fracture height. This method is already implemented in gOcad-SKUA software as a macro that extrudes planes of a single fracture family (i.e. all the red fractures in AP3) vertically into a bounded volume (Fig. 15). More developments are in process to generate oblique planes and to be able to extrude planes in portions of the fracture family.

V] Conclusions

In this paper a new method to predict the geometry of a natural fracture network using the multiple-point statistic algorithm is presented. The method allows to provide a realistic non-stationary fracture network arrangement in 2D based on the use of multiple, simplified, small training images capturing the natural fracture attributes in specific zones defined by a probability map. Probability maps are adaptable and follow geological rules of fracture type and arrangement distribution specific to various tectonic contexts (i.e. faulting, folding and poor deformation context/no fault, no folds). We developed methods to be able to consider transition zones into the probability maps (e.g. zones far from hard data) that allow simulating fracture network geometry at a larger scale (i.e. reservoir scale).

The realisation obtained from 2D MPS constitutes a statistical laboratory close enough to the reality to be tested in terms of fracture mechanical parameters and response to flow.

Comparison between mechanical aperture calculation, fluid flow simulations conducted on both "reality" fracture network interpretations performed on drone imagery and series of MPS realisations gives similar results.

The method proposed here is applicable to all rock types and to a wide range of tectonic contexts. Initially calibrated using outcrop data, the method is fully adaptable to the subsurface in order to better characterise fractures in water, heat or hydrocarbon reservoirs. The challenge there, remains on the definition of the different training images on which is simulation is based. Very few data are generally available in the subsurface and geological rules need to be found to define the geological characteristics of the fracture network (orthogonal or conjugate network) and the associated fracture attributes (length, height, spacing, density, topology).

Acknowledgments

The authors want to thank ENI S.P.A. for the financial support of this research. Silvia Mittempergher from the University of Milano Bicocca is acknowledged for providing the code extracting segments from pixelated images. We would like also to thank the entire SEFRAC group for their interest in developing this method and for their valuable geological advices. Acknowledgements are extended to Philippe Renard from the University of Neuchâtel, to Hadi Hajibeygi from TU Delft and to Wilfried Tsoblefack from Paradigm Geo for the constructive discussions we had together. Prof. Hilario Bezerra from the Universidade Federal do Rio Grande do Norte is acknowledged for providing datasets concerning Apodi area and for his advises on the local geology. We would like to thank Jan Kees Blom from the TU Delft for the improvement he provided to this manuscript.

Appendix A

Solid Earth Discuss., https://doi.org/10.5194/se-2018-106
Manuscript under review for journal Solid Earth
Discussion started: 11 October 2018

676 In the Barton-Bandis stress aperture model, the hydraulic fracture aperture is a function of
677 local stresses, shear displacement, initial roughness of the fracture and mechanical properties
678 of the rock. A set of empirical functions for the mechanical aperture was defined by (Barton,
679 1982). (Olsson and Barton, 2001) defined the hydraulic aperture as a function of the
680 mechanical aperture. The initial mechanical aperture is given by the following relation from
681 which the mechanical aperture is a function of the Joint Roughness Coefficient (JRC), Joint
682 Compressive Strength (JCS) and uniaxial compressive strength (in MPa).

$$E_0 = \frac{JRC}{5}\left(0.2\frac{\sigma_c}{JCS} - 0.1\right)$$

683

684 The JRC is a measure of the relative roughness of the rock fracture surface and is commonly
685 measured using a Barton comb. The JCS can be measured in the field using Schmidt hammer
686 rebound measurements. The joint compressive strength (in MPa) is a mechanical property of
687 the rock. For our simulations, we set JRC = 15 and JCS equal to the uniaxial compressive
688 strength of 120 MPa, so that we obtain an initial unstressed mechanical aperture of 0.3 mm
689 which is independent of length or network geometry. This is valid for an un-weathered
690 fracture where the initial unstressed aperture is only a function of roughness. The mechanical
691 aperture is a function of the normal stress, initial stiffness and the maximum closure.

$$E_n = E_0 - \left(\frac{1}{v_m} + \frac{K_{ni}}{\sigma_n}\right)^{-1}$$

692

693 The initial stiffness (in MPa/mm) and maximum closure (in mm) are functions of the JRC,
694 JCS and the initial mechanical aperture.

$$K_{ni} = (-7.15) + 1.75JRC + 0.02\left(\frac{JCS}{E_0}\right)$$

695

$$v_m = A + B(JRC) + C\left(\frac{JCS}{E_0}\right)^D$$

696

Solid Earth Discuss., https://doi.org/10.5194/se-2018-106
Manuscript under review for journal Solid Earth
Discussion started: 11 October 2018

697 The values of the coefficients in the maximum closure equation, vary according to cycles of
698 loading. These coefficients have been given by Asadollahi et al., (2010) and we use the
699 corresponding values for the third cycle where A = -0.1032 ± 0.0680, B = -0.0074 ± 0.0039,
700 C = 1.1350 ± 0.3261 and D = -0.2510 ± 0.1029. The hydraulic aperture, *e* (in mm) is a
701 function of shear displacement, normal stress, peak shear displacement and mobilized fracture
702 roughness. The shear displacement is obtained numerically. The domain for which $0.75 \leq u_s / u_{peak} \leq 1$ is calculated using linear interpolation (Olsson and Barton, 2001).

703

$$e = \begin{cases} for \dfrac{u_s}{u_{peak}} \leq 0.75 ; \dfrac{E_n^{\,2}}{JRC^{2.5}} \\ for \dfrac{u_s}{u_{peak}} \geq 1; \sqrt{E_n}\, JRC_{mob} \end{cases}$$

704

705 The peak displacement and mobilized JRC is obtained using the following relations.

$$u_{\text{peak}} = 0.0077 L^{0.45} \left(\frac{\sigma_n}{\text{JCS}}\right)^{0.34} \cos\left(\text{JRClog}_{10}\left[\frac{\text{JCS}}{\sigma_n}\right]\right)$$

706

$$JRC_{mob} = JRC\left[\frac{u_s}{u_{peak}}\right]^{-0.381}$$

707 The peak displacement is a function of JRC, JCS, normal stress and the block size, L (in
708 metres). Within a fracture network, the block size is the spacing of the fracture set intersecting
709 the fracture of interest (Barton, 1982). The mobilized JRC indicates the shear activated
710 fracture wall roughness and is dependent upon the ratio between shear displacement and peak
711 shear displacement.

712

713

714

715

716

Solid Earth Discuss., https://doi.org/10.5194/se-2018-106
Manuscript under review for journal Solid Earth
Discussion started: 11 October 2018

Figure captions

Figure 1: Direct Sampling method workflow applied to fracture network modelling (modified from (modified from (Meerschman et al., 2013).

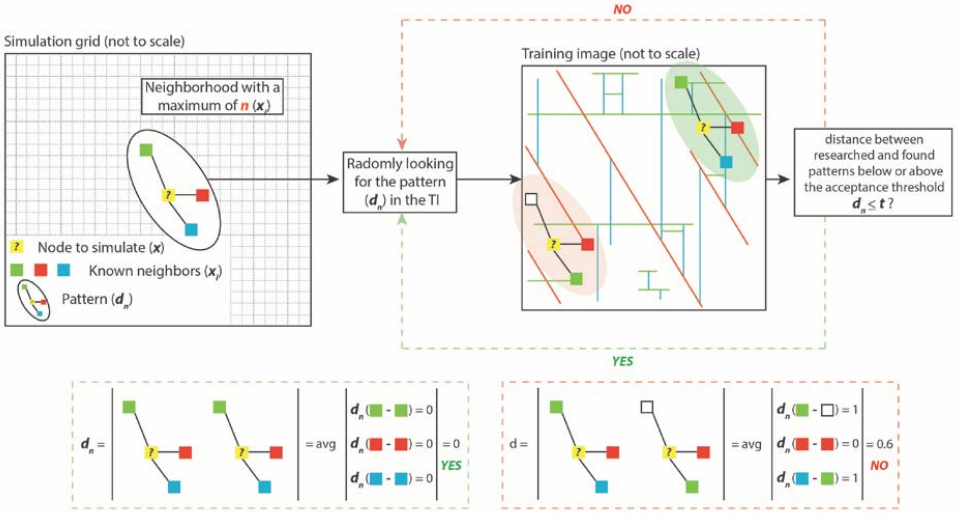

Figure 2: Location of the area of interest and of the studied pavements near Apodi area (red star).

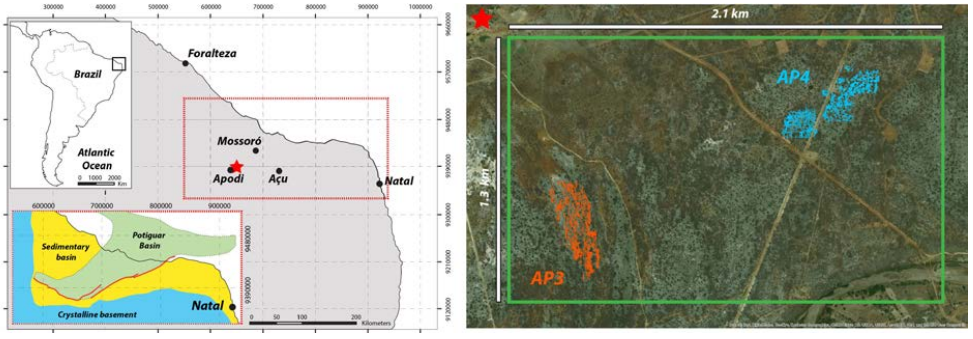

Solid Earth Discuss., https://doi.org/10.5194/se-2018-106
Manuscript under review for journal Solid Earth
Discussion started: 11 October 2018

729 **Table 1:** Outcrop characteristics and fracture parameters collected in AP3 and AP4

AP3 outcrop																				
Localisation (WGS84 UTM Z24S)		Orientation	Dimension		Fractures proportion (of the whole fracture population)														Fracture length	
X	Y		NS (m)	EW (m)	Set 1 (N135-N165)					Set 2 (N000-N010/N170-180)					Set3 (N075-N105)					Min (m)	Max (m)
650601	9387908	NNW-SSE	600	300	30%					52%					18%					2,21	123
					Elementary zone 1	Elementary zone 2	Elementary zone 3	Elementary zone 4	Elementary zone 5	Elementary zone 1	Elementary zone 2	Elementary zone 3	Elementary zone 4	Elementary zone 5	Elementary zone 1	Elementary zone 2	Elementary zone 3	Elementary zone 4	Elementary zone 5		
					60%	26%	18%	70%	87%	37%	14%	80%	23%	13%	3%	60%	2%	7%	0%		

AP4 outcrop														
Localisation (WGS84 UTM Z24S)		Orientation	Dimension		Fractures proportion (of the whole fracture population)									Fracture length	
X	Y		NS (m)	EW (m)	Set 1 (N135-N165)			Set 2 (N000-N010/N170-180)			Set3 (N075-N105)			Min (m)	Max (m)
652032	9388508	NE-Sw	400	500	20%			40%			40%			1	186
					Elementary zone 6	Elementary zone 7	Elementary zone 8	Elementary zone 6	Elementary zone 7	Elementary zone 8	Elementary zone 6	Elementary zone 7	Elementary zone 8		
					8%	20%	10%	43%	45%	53%	49%	35%	37%		

730

731

732

733

734

735

736

737

738

739

740

741

Figure 3: data acquired in the area of interest in pavements AP3. A) ortho-rectified high-resolution pavement aerial images acquired with a drone, B) fracture interpretation on ortho-rectified images, C) fracture orientation calculated from the north in GIS-based environment. Corresponding rose diagram for both outcrops, D) length of each fracture trace and E) fracture topology relationship for each pavement observed on fracture network interpretation.

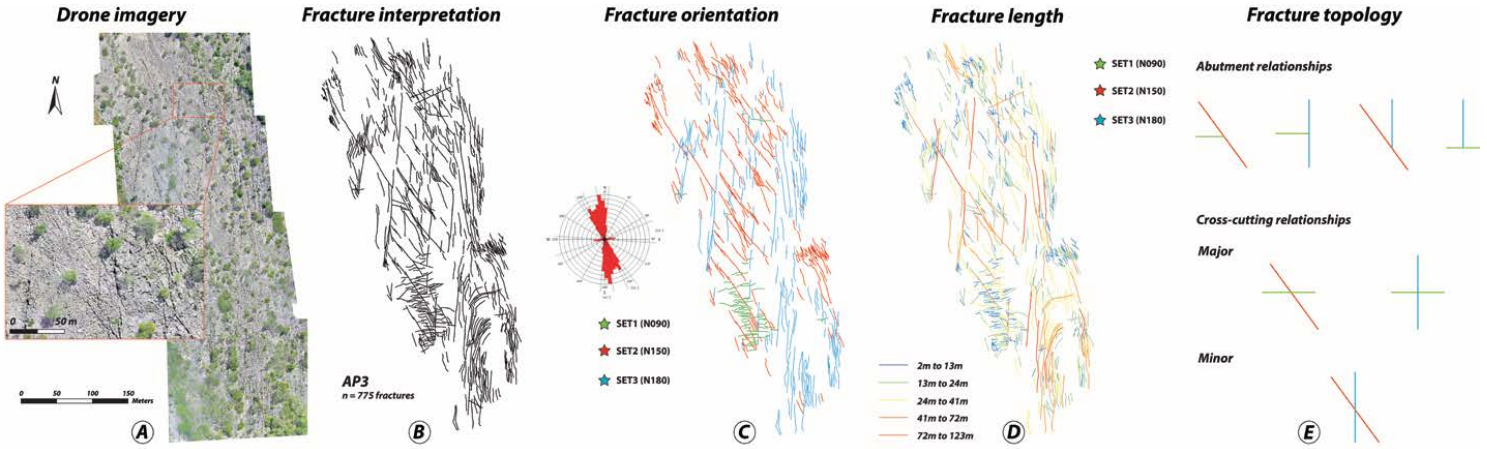

Figure 4: data acquired in the area of interest in pavements AP4. F) ortho-rectified high-resolution pavement aerial images acquired with a drone, G) fracture interpretation on ortho-rectified images, H) fracture orientation calculated from the north in GIS-based environment. Corresponding rose diagram for both outcrops, I) length of each fracture trace and J) fracture topology relationship for each pavement observed on fracture network interpretation

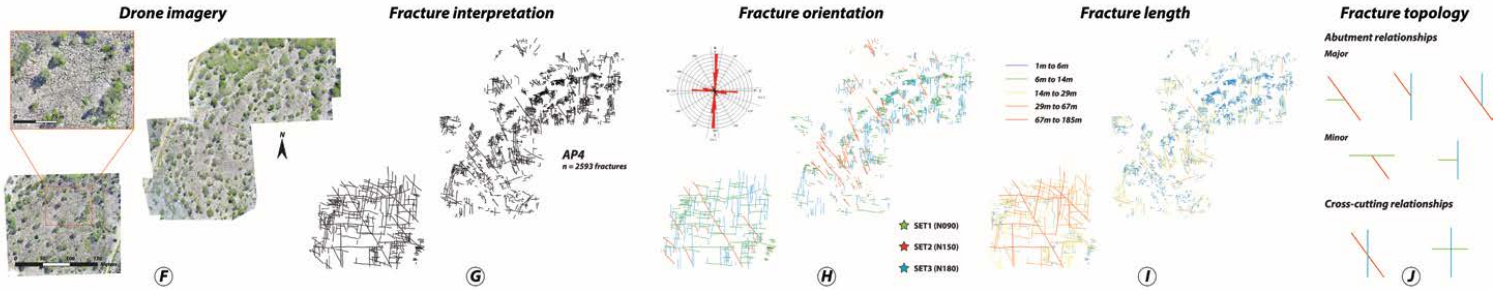

Solid Earth Discuss., https://doi.org/10.5194/se-2018-106
Manuscript under review for journal Solid Earth
Discussion started: 11 October 2018

760 **Figure 5:** A) Partitioning of AP3 in 5 elementary zones (EZ). This partition is defined (with
761 respect to fracture orientation (fracture facies), fracture density and geometry variability over
762 the entire simulation domain. B) probability map and associated statistics for each EZ. C)
763 training images associated with the partition of AP3. In each EZ, the corresponding training
764 image has a probability (pTI) of 1 to be used. In this zone the other training images are not
765 used (pTI = 0). D) hard conditioning data for AP3. All the fractures longer than 40 m are
766 considered deterministically in the simulation process

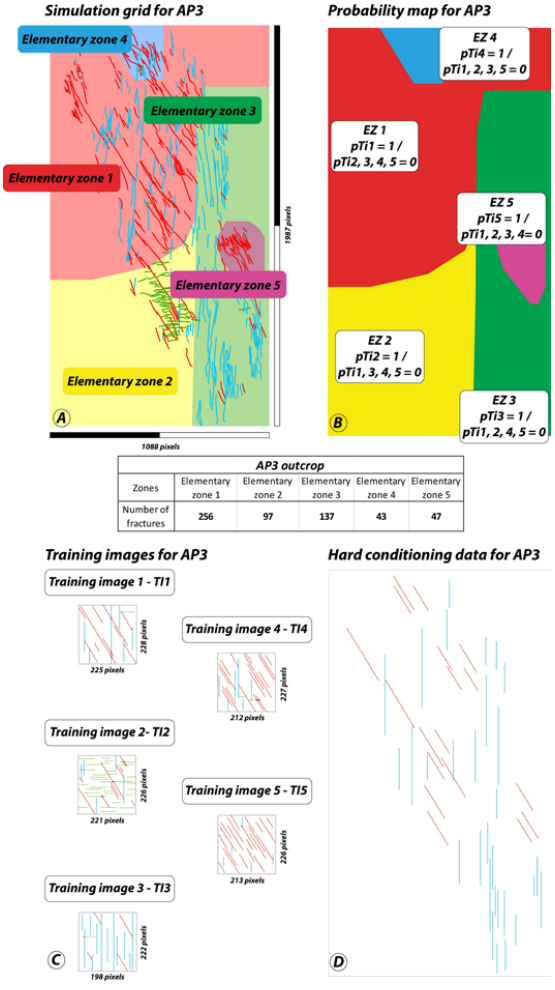

767

Solid Earth Discuss., https://doi.org/10.5194/se-2018-106
Manuscript under review for journal Solid Earth
Discussion started: 11 October 2018

768 **Figure 6:** comparison between results obtained without constraining the topology and with
769 topological facies constraints.

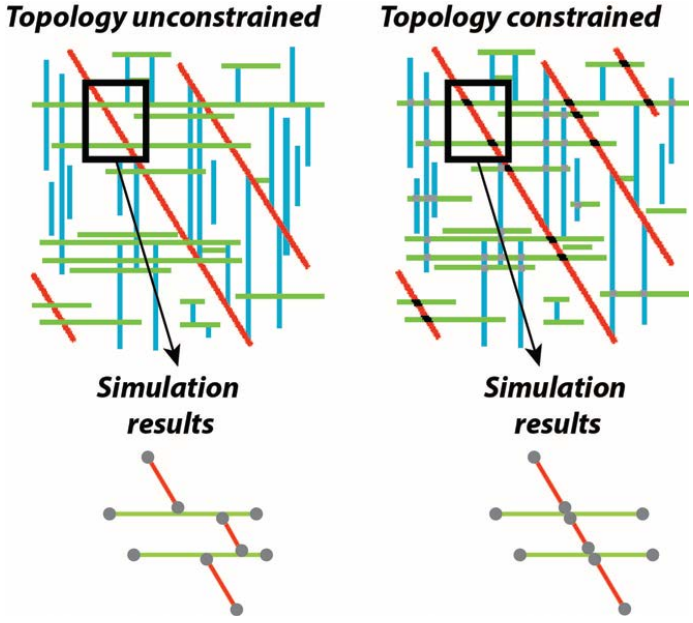

770

771

772 **Figure 7:** visual comparison between: A) the reference fracture network interpretation (AP3),
773 B) the extraction of the longer segments (50 fracture longer than 40m), C) a simulation
774 conditioned by the long segments, D) a simulation not conditioned by the long segments

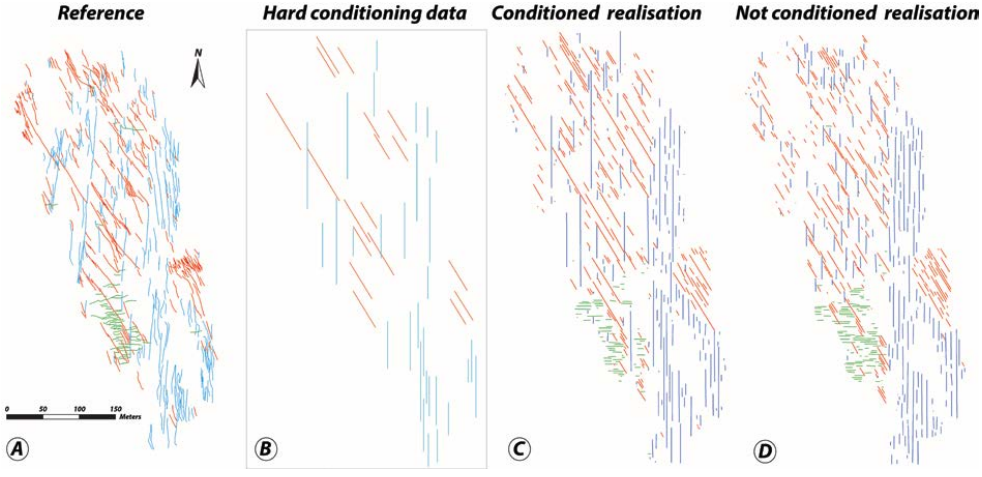

775

Solid Earth Discuss., https://doi.org/10.5194/se-2018-106
Manuscript under review for journal Solid Earth
Discussion started: 11 October 2018

Table 2: simulation parametrisation, models set-ups and duration of each run.

Tested parametrisation	Number of neighbours influence							Number of neighbours + Acceptance threshold						
Realisation name	SIM1	SIM2	SIM3	SIM4	SIM5	SIM6	SIM7	SIM8	SIM9	SIM10	SIM11	SIM12	SIM13	SIM14	SIM15
Simulation parameters	A. th. = 5% N. = 10 Scan= 25%	A. th. = 5% N. = 20 Scan= 25%	A. th. = 5% N. = 30 Scan= 25%	A. th. = 5% N. = 40 Scan= 25%	A. th. = 5% N. = 50 Scan= 25%	A. th. = 5% N. = 75 Scan= 25%	A. th. = 5% N. = 100 Scan= 25%	A. th. = 4% N. = 40 Scan= 25%	A. th. = 3% N. = 40 Scan= 25%	A. th. = 2% N. = 40 Scan= 25%	A. th. = 1% N. = 40 Scan= 25%	A. th. = 4% N. = 50 Scan= 25%	A. th. = 3% N. = 50 Scan= 25%	A. th. = 2% N. = 50 Scan= 25%	A. th. = 1% N. = 50 Scan= 25%
Simulation duration	22"	19"	33"	36"	55"	101"	136"	52"	52"	90"	95"	56"	76"	76"	121"

Tested parametrisation	Number of neighbours + Acceptance threshold + % TI scan												Optimisation
Group	Group 1				Group 2				Group3				
Realisation name	SIM16	SIM17	SIM18	SIM19	SIM20	SIM21	SIM22	SIM23	SIM24	SIM25	SIM26	SIM27	OPT1
Simulation parameters	A. th. = 3% N. = 40 Scan= 50%	A. th. = 2% N. = 40 Scan= 50%	A. th. = 3% N. = 50 Scan= 50%	A. th. = 2% N. = 50 Scan= 50%	A. th. = 3% N. = 40 Scan= 75%	A. th. = 2% N. = 40 Scan= 75%	A. th. = 3% N. = 50 Scan= 75%	A. th. = 2% N. = 50 Scan= 75%	A. th. = 3% N. = 40 Scan= 100%	A. th. = 2% N. = 40 Scan= 100%	A. th. = 3% N. = 50 Scan= 100%	A. th. = 2% N. = 50 Scan= 100%	Custom
Simulation duration	80"	148"	123"	124"	105"	196"	152"	154"	104"	203"	150"	149"	151"

Table 3: Comparison between the total amount of segments interpreted in the reference outcrop and in the different sets of simulations (tested parametrisation). Evaluation of the results in terms of satisfactory (green symbol), acceptable (orange symbol) or non-satisfactory (red symbol)

				Results evaluation		
	Reference outcrop	Tested Parametrisation	Number of tested configurations	✓	≈	✗
Total segments	562	Influence of the number of neighbours	n=7	1	1	5
		Number of neighbours + Acceptance threshold	n=8	3	2	3
		Number of neighbours + Acceptance threshold + % TI scan	n=12	5	6	1

Solid Earth Discuss., https://doi.org/10.5194/se-2018-106
Manuscript under review for journal Solid Earth
Discussion started: 11 October 2018

794 **Table 4**: results of the sensitivity analysis on the influence of the number of neighbours. The
795 table presents the number of segments per simulation zone for AP3 (used as reference). Red
796 symbols show a total amount of segments of the considered set in the considered zone
797 deviating to more than 20% from the reference case. Yellow symbols show a deviation of
798 more than 10% from the reference case. Green symbols do not deviate significantly from the
799 reference outcrop interpretation.

			Number of neighbours						
		Reference	SIM1	SIM2	SIM3	SIM4	SIM5	SIM6	SIM7
		Segments per parts							
Zone TI1	Set1	156	✗	≈	≈	✗	✗	✗	✗
	Set2	95	✗	✗	≈	✗	✗	✗	✗
	Set3	6	✗	✗	✗	✗	✗	✗	✗
Zone TI2	Set1	22	✗	✗	✗	✗	✗	✗	≈
	Set2	12	✗	✗	✓	✗	✗	✗	✗
	Set3	57	✗	≈	✓	✓	✓	≈	✓
Zone TI3	Set1	20	✗	✓	✗	✗	✗	✗	✗
	Set2	113	✗	≈	✓	≈	≈	✗	✗
	Set3	2	✗	✗	✗	≈	≈	✗	✗
Zone TI4	Set1	25	✗	✗	✗	✓	✓	≈	✗
	Set2	10	✓	✓	✓	✓	≈	≈	≈
	Set3	3	✗	✗	✗	✗	✗	✗	≈
Zone TI5	Set1	39	✓	≈	✗	✗	✗	✗	✗
	Set2	2	✗	✗	✗	✗	✓	✓	≈
	Set3	0	✓	✓	✓	✓	✓	✓	✓
		Satisfactory total	No	Yes	Yes	No	No	No	No
		# satisfactory	3	3	5	4	4	2	4
		# acceptable	0	4	2	2	3	3	2
		# not acceptable	12	8	8	9	8	10	9

800
801
802
803
804
805
806
807

Solid Earth Discuss., https://doi.org/10.5194/se-2018-106
Manuscript under review for journal Solid Earth
Discussion started: 11 October 2018

Table 5: results of the sensitivity analysis on the influence of the number of neighbours and of the variation of the acceptance threshold. The colour code is the same as the one used in table 4.

			Number of neighbours + Acceptance threshold							
		Reference	SIM8	SIM9	SIM10	SIM11	SIM12	SIM13	SIM14	SIM15
		Segments per parts								
Zone TI1	Set1	156	✓	✓	≈	≈	✗	✓	✓	✓
	Set2	95	✗	✗	✗	✗	✗	✗	✗	✗
	Set3	6	✗	✗	✗	✗	✗	✗	✗	✗
Zone TI2	Set1	22	✗	✗	✗	✗	✗	✗	✗	✗
	Set2	12	≈	≈	✓	✓	✗	✗	✗	✗
	Set3	57	✓	✓	✗	✗	✓	✓	✓	≈
Zone TI3	Set1	20	✗	✗	✓	✓	✗	✗	✗	✗
	Set2	113	✓	✓	≈	≈	≈	✓	✓	≈
	Set3	2	≈	≈	✓	✓	≈	✗	✗	✓
Zone TI4	Set1	25	✓	✓	✗	✗	✓	✓	✓	✓
	Set2	10	✗	✗	≈	≈	≈	≈	≈	✓
	Set3	3	✗	✗	✗	✗	✗	✗	✗	✗
Zone TI5	Set1	39	✗	✗	✗	✗	✗	✗	✗	✗
	Set2	2	≈	≈	≈	≈	✓	≈	≈	≈
	Set3	0	✓	✓	✓	✓	✓	✓	✓	✓
		Satisfactory total	Yes	Yes	Yes	Yes	No	No	No	Yes
		# satisfactory	5	5	4	4	4	5	5	5
		# acceptable	3	3	4	4	6	2	2	3
		# not acceptable	7	7	7	7	9	8	8	7

Table 6: results of the sensitivity analysis on the influence of the number of neighbours, of the variation of the acceptance threshold and of the variation of the percentage of the scanned fraction of the training image. The colour code is the same as the one used in table

			Number of neighbours + Acceptance threshold + % TI scan											Optimisation
			Group 1				Group 2			Group3				
		Reference	SIM16	SIM17	SIM18	SIM19	SIM20	SIM21	SIM22	SIM23	SIM24	SIM25	SIM26	SIM27	OPT1
		Segments per parts													
Zone TI1	Set1	156		✓	✓	✓	✓	✗	✓	✓	✓	✗	✓	✓	✗
	Set2	95		✗	✗	✗	✗	≈	✗	✗	✗	≈	✗	✗	✓
	Set3	6		✗	✗	✗	✗	✗	✗	✗	✗	✗	✗	✗	✓
Zone TI2	Set1	22		✗	✗	✗	✗	✗	✗	✗	✗	✗	✗	✗	✗
	Set2	12		✗	✗	✗	✗	✗	✗	✗	✓	✗	✓	✓	✓
	Set3	57		✓	✓	✓	✓	≈	✓	✓	✓	≈	✓	✓	≈
Zone TI3	Set1	20		✗	✗	✗	✓	✗	✗	✗	≈	✗	✓	✓	✗
	Set2	113		✓	✓	✓	≈	✓	✓	✓	✓	✓	≈	≈	✓
	Set3	2		≈	≈	≈	✗	✓	✓	✓	≈	≈	✗	✗	✗
Zone TI4	Set1	25		✗	✗	✗	≈	✗	✓	✓	✗	✗	≈	≈	✗
	Set2	10		✓	✓	✓	≈	✓	✓	✓	✗	≈	✓	✓	✓
	Set3	3		✗	✗	✗	✗	✗	✗	✗	✗	≈	✗	✗	✓
Zone TI5	Set1	39		≈	≈	≈	✗	✗	✗	✗	✓	≈	✗	✗	≈
	Set2	2		≈	≈	≈	✗	✗	✓	✓	≈	≈	✓	✓	✓
	Set3	0		✓	✓	✓	✓	✓	✓	✓	✓	✓	✓	✓	✓
		Satisfactory total		Yes	Yes	Yes	No	No	Yes	Yes	Yes	Yes	Yes	Yes	Yes
		# satisfactory		5	5	5	4	4	8	8	6	2	7	7	8
		# acceptable		3	3	3	3	2	0	0	3	7	2	2	2
		# not acceptable		7	7	7	8	9	7	7	6	6	6	6	5

Solid Earth Discuss., https://doi.org/10.5194/se-2018-106
Manuscript under review for journal Solid Earth
Discussion started: 11 October 2018

816 **Figure 8:** fracture length distributions tested during the sensitivity analysis. A) fracture length
817 distribution for SIM1 to SIM7, B) fracture length distribution for SIM10, SIM12, SIM13,
818 SIM15 and C) fracture length distribution for SIM16, SIM17, SIM20, SIM21, SIM22, SIM24,
819 SIM5, SIM26.

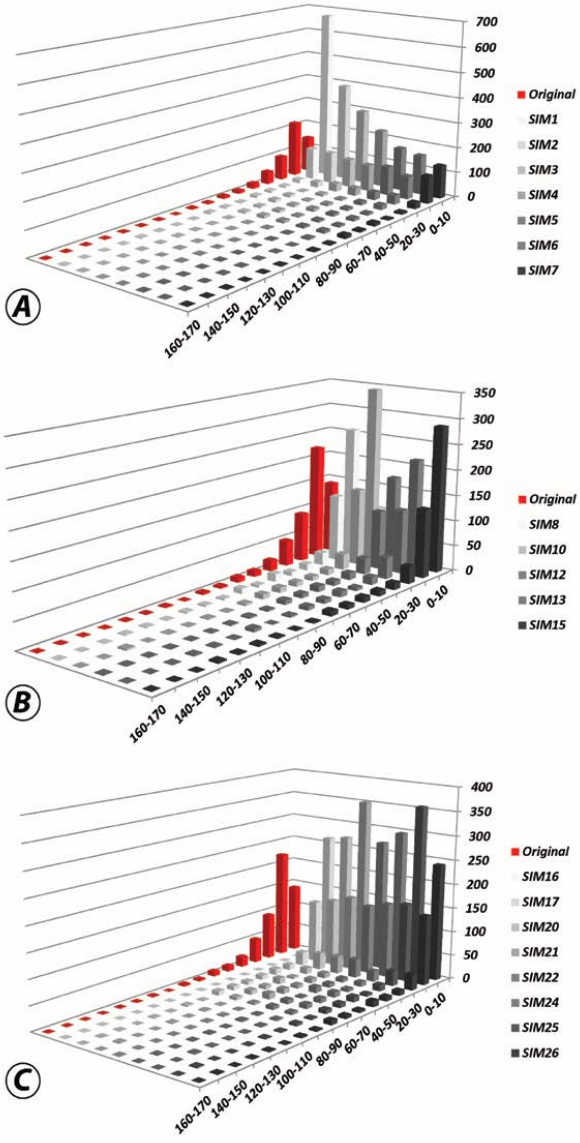

820

Solid Earth Discuss., https://doi.org/10.5194/se-2018-106
Manuscript under review for journal Solid Earth
Discussion started: 11 October 2018

821 **Figure 9:** comparison of the training images 1, 3 and 4 used during the sensitivity analysis
822 (27 simulations) and their modification for SIM 3

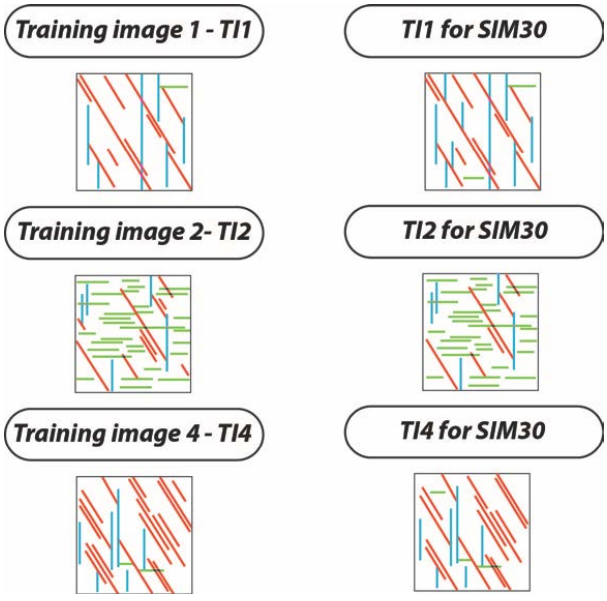

823
824
825
826
827
828
829
830
831
832
833
834
835
836

Solid Earth Discuss., https://doi.org/10.5194/se-2018-106
Manuscript under review for journal Solid Earth
Discussion started: 11 October 2018

837 **Figure 10:** A) Partitioning of AP4 in 3 EZ. B) probability map and associated statistics for
838 each EZ. C) training images associated with the partition of AP4. D) hard conditioning data
839 for AP4

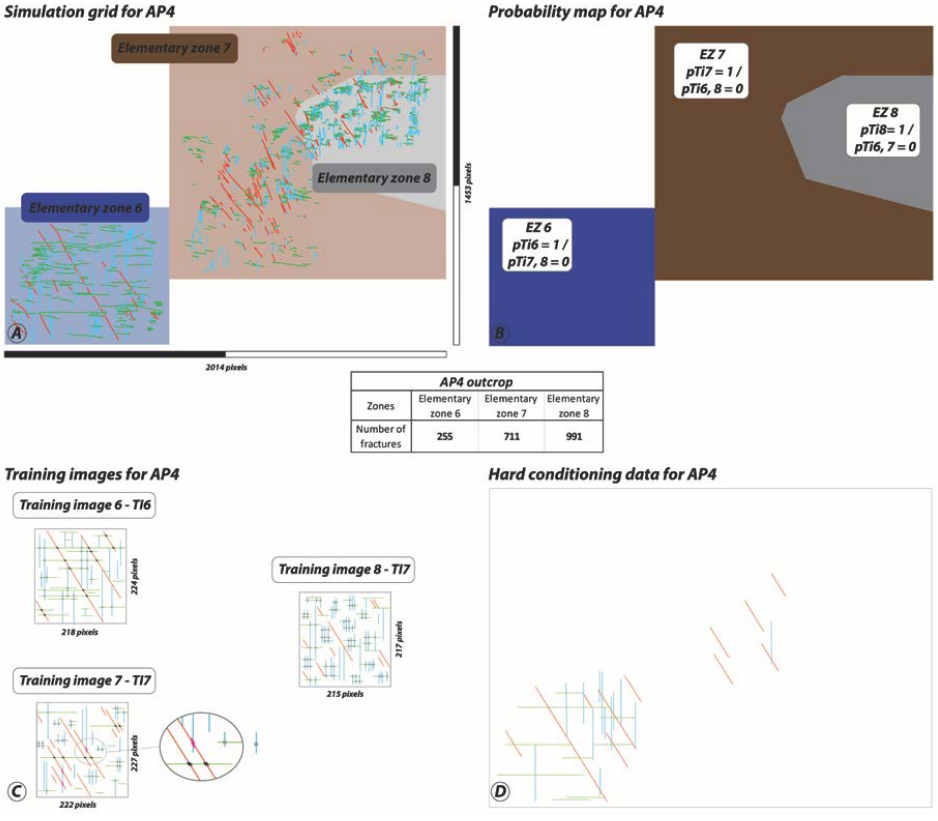

840
841
842
843
844
845
846
847
848

Solid Earth Discuss., https://doi.org/10.5194/se-2018-106
Manuscript under review for journal Solid Earth
Discussion started: 11 October 2018

849 **Figure 11:** comparison of the AP4 original outcrop with a MPS simulated version AP4-1

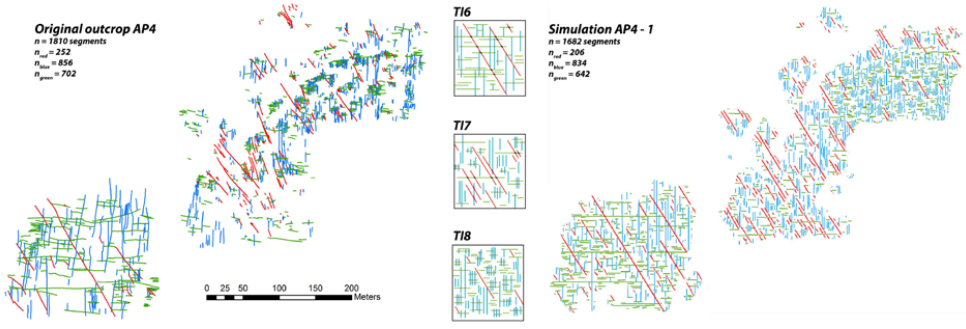

850

851

852

853

854

855

856

857

858

859

860

861

862

863

864

865

866

867

868

Solid Earth Discuss., https://doi.org/10.5194/se-2018-106
Manuscript under review for journal Solid Earth
Discussion started: 11 October 2018

869 **Figure 12:** smooth probability map at the reservoir scale (combination of AP3 and AP4). A)
870 Relative position of AP3 and AP4 outcrops. B) Apodi fault added into the area of interest.
871 Extension of the probability map regions in AP3 and AP4 without geological drivers C) and
872 with the influence of the Apodi fault D). Probability maps with smooth transition zones
873 without geological drivers E) and with the influence of the Apodi fault F).

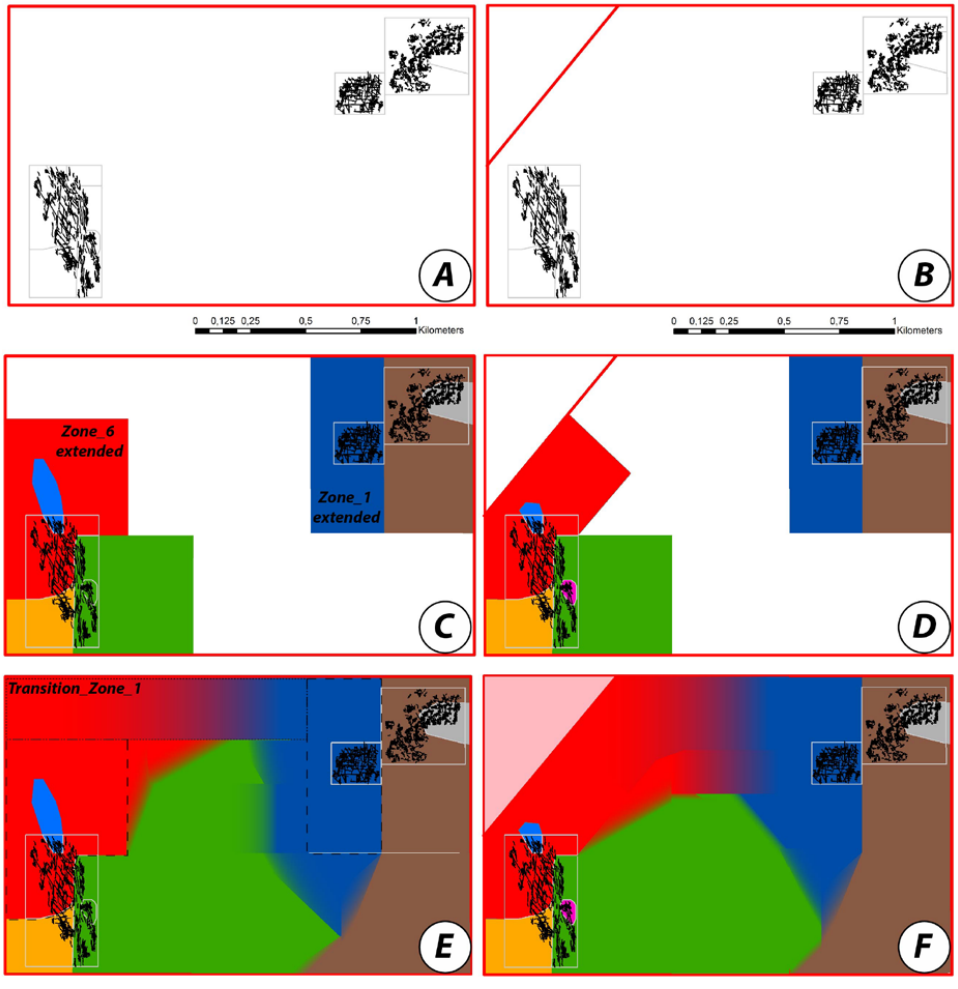

874
875
876

Solid Earth Discuss., https://doi.org/10.5194/se-2018-106
Manuscript under review for journal Solid Earth
Discussion started: 11 October 2018

877 **Figure 13:** principle and parameters used in the calculation of stress-induced mechanical and
878 hydraulic aperture using the Barton-Bandis approach (modified from (Bisdom, 2016)). The
879 left hand-side sketch represents the initial stage where the fracture is not submitted to stress
880 (aperture is constant). The right hand side sketch represents the same configuration submitted
881 to stress (aperture is not constant).

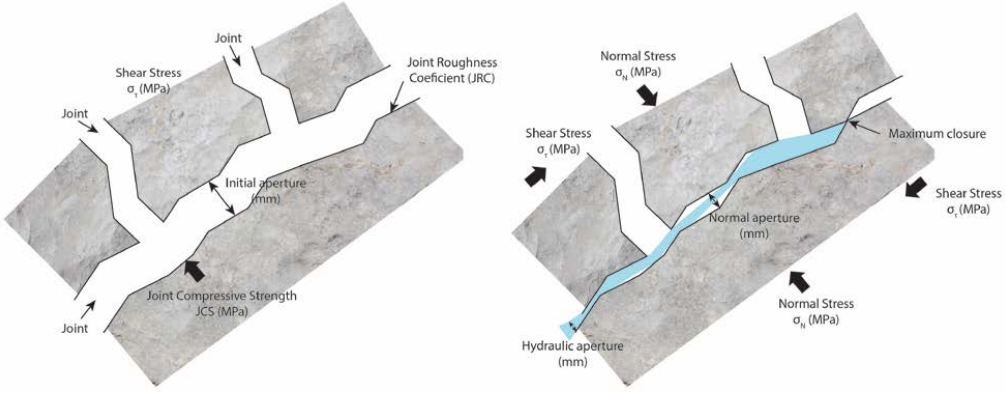

882
883
884
885
886
887
888
889
890
891
892
893
894
895

Solid Earth Discuss., https://doi.org/10.5194/se-2018-106
Manuscript under review for journal Solid Earth
Discussion started: 11 October 2018

Figure 14: Mechanical and hydraulic aperture calculated in the original outcrop (AP3) and in four selected MPS simulations

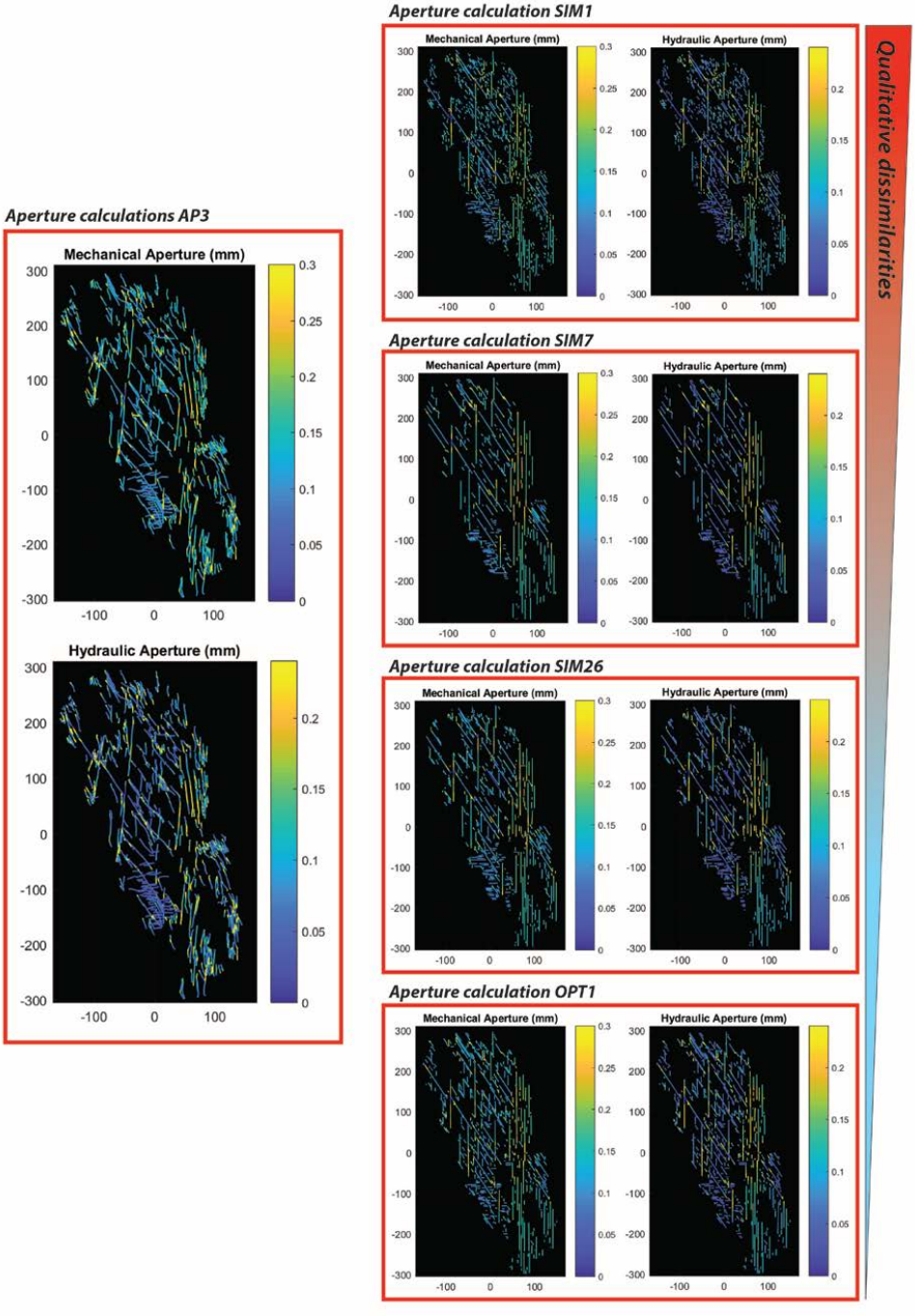

Solid Earth Discuss., https://doi.org/10.5194/se-2018-106
Manuscript under review for journal Solid Earth
Discussion started: 11 October 2018

Figure 15: fracture network extrusion in 3D. The method consists of identifying the different fracture units (FU) on which the fracture height is supposed to be constant (A). This method requires one simulation per top fracture unit (SIM SLICES). (B) is a 3D DFN based on the hypothetical case (A) and realised in gOcad software. (C) is a cross section realised in the centre of the 3D model in the E-W direction.

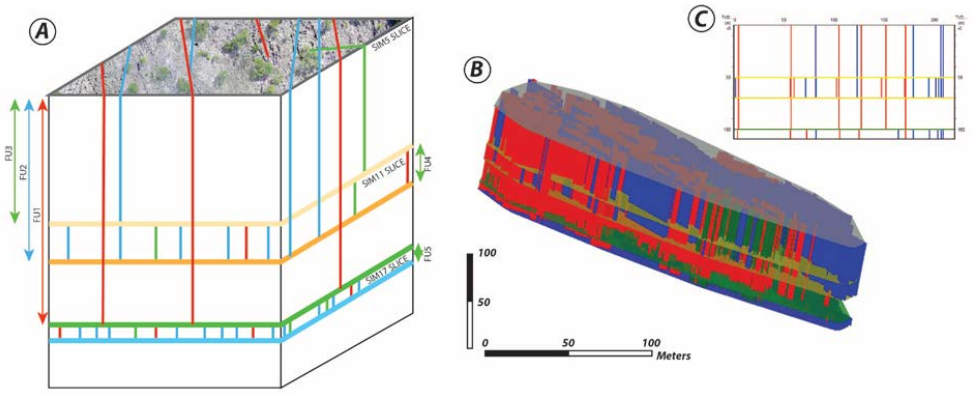

References

Agar, S. M. and Geiger, S.: Fundamental controls on fluid flow in carbonates: current workflows to emerging technologies, Geological Society, London, Special Publications, 406, 60, 2015.

Angelim, L. A. A., Medeiros, V. C., and Nesi, J. R.: Mapa geológico do Estado do Rio Grande do Norte, CPRM/FAPERN, Recife, Projeto Geologia e Recursos Minerais do Estado do Rio Grande do Norte, 2006.

Barton, N.: Modelling rock joint behaviour from in situ block tests: Implications for nuclear waste repository design, Office of Nuclear Waste Isolation, Columbus, OH, USA, 1982.

Barton, N. and Bandis, S.: Some effects of scale on the shear strength of joints, International Journal of Rock Mechanics and Mining Sciences & Geomechanics Abstracts,, 17, 5, 1980.

Bemis, S. P., Micklethwaite, S., Turner, D., James, M. R., Akciz, S., Thiele, S. T., and Bangash, H. A.: Ground-based and UAV-Based photogrammetry: A multi-scale, high-resolution mapping tool for structural geology and paleoseismology, Journal of Structural Geology, 69, 163-178, 2014.

Berkowitz, B.: Characterizing flow and transport in fractured geological media: A review, Advances in Water Resources, 25, 861-884, 2002.

Bertotti, G., de Graaf, S., Bisdom, K., Oskam, B., Vonhof, H. B., Bezerra, F. H. R., Reijmer, J. J. G., and Cazarin, C. L.: Fracturing and fluid-flow during post-rift subsidence in carbonates of the Jandaira Formation,Potiguar Basin,NE Brazil, Basin Research, 29, 18, 2017.

Bisdom, K.: Burial-related fracturing in sub-horizontal and folded reservoirs - Geometry, geomechanics and impact on permeability, Doctorate, Technische Universiteit Delft, 2016.

Bisdom, K., Gauthier, B. D. M., Bertotti, G., and Hardebol, N. J.: Calibrating discrete fracture-network models with a carbonate three-dimensional outcrop fracture network: Implications for naturally fractured reservoir modeling, AAPG Bulletin, 98, 1351-1376, 2014.

Bisdom, K., Nick, H. M., and Bertotti, G.: An integrated workflow for stress and flow modelling using outcrop-derived discrete fracture networks, Computers & Geosciences, 103, 21-35, 2017.

Bruna, P.-O., Guglielmi, Y., Viseur, S., Lamarche, J., and Bildstein, O.: Coupling fracture facies with in-situ permeability measurements to generate stochastic simulations of tight carbonate aquifer properties: Example from the Lower Cretaceous aquifer, Northern Provence, SE France, Journal of Hydrology, 529, Part 3, 737-753, 2015.

Bruna, P.-O., Hardebol, N., Bisdom, K., Straubhaar, J., Mariethoz, G., and Bertotti, G.: 2D to 3D fracture network detection and forecasting in a carbonate reservoir analogue using Multiple Point Statistics (MPS). ExCEL London2017.

Bruna, P.-O., Prabhakaran, R., Bertotti, G., Mittempergher, S., Succo, A., Bistacchi, A., Storti, F., and Meda, M.: Multiscale 3D prediction of fracture network geometry and fluid flow efficiency in folded carbonate reservoir analogues; Case study of the Island of Pag (Croatia). Muscat, Oman, 5-7 February 2018 2018.

Chopra, S. and Marfurt, K. J.: Volumetric curvature attributes for fault/fracture characterization, First Break, 25, 12, 2007.

Chugunova, T., Corpel, V., and Gomez, J.-P.: Explicit fracture network modelling: from multiple point statistics to dynamic simulation, Mathematical Geosciences, 49, 13, 2017.

Claes, H., Degros, M., Soete, J., Claes, S., Kele, S., Mindszenty, A., Török, Á., El Desouky, H., Vanhaecke, F., and Swennen, R.: Geobody architecture, genesis and petrophysical characteristics of the Budakalász travertines, Buda Hills (Hungary), Quaternary International, 437, 107-128, 2017.

968 Corradetti, A., Tavani, S., Parente, M., Iannace, A., Vinci, F., Pirmez, C., Torrieri, S., Giorgioni,
969 M., Pignalosa, A., and Mazzoli, S.: Distribution and arrest of vertical through-going joints in a
970 seismic-scale carbonate platform exposure (Sorrento peninsula, Italy): insights from
971 integrating field survey and digital outcrop model, Journal of Structural Geology, doi:
972 https://doi.org/10.1016/j.jsg.2017.09.009, 2017a. 2017a.
973 Corradetti, A., Tavani, S., Russo, m., Arbues, P. C., and Granado, P.: Quantitative analysisi of
974 folds by means of orthorectified photogrammetric 3D models: A case study from Mt. Catria,
975 Northern Apennines, Italy, The photogrammetric record, doi: 10.1111/phor.12212, 2017b.
976 17, 2017b.
977 Costa de Melo, A. C., de Castro, D. L., Bezerra, F. H. R., and Bertotti, G.: Rift fault geometry
978 and evolution in the Cretaceous Potiguar Basin (NE Brazil) based on fault growth models,
979 Journal of South American Earth Sciences, 71, 96-107, 2016.
980 de Brito Neves, B. B., Fuck, R. A., Cordani, U. G., and Thomaz F°, A.: Influence of basement
981 structures on the evolution of the major sedimentary basins of Brazil: A case of tectonic
982 heritage, Journal of Geodynamics, 1, 495-510, 1984.
983 Deutsch, C. V. and Journel, A. G.: GSLIB : Geostatistical software library and user's guide,
984 New York, 1997.
985 Faulkner, D. R., Jackson, C. A. L., Lunn, R. J., Schlische, R. W., Shipton, Z. K., Wibberley, C. A.
986 J., and Withjack, M. O.: A review of recent developments concerning the structure,
987 mechanics and fluid flow properties of fault zones, Journal of Structural Geology, 32, 1557-
988 1575, 2010.
989 Gringarten, E. and Deutsch, C. V.: Methodology for Variogram Interpretation and Modeling
990 for Improved Reservoir Characterization, SPE Annual Technical Conference and Exhibition,
991 Texas, Houston, 1999.
992 Gringarten, E. and Deutsch, C. V.: Teacher's Aide Variogram Interpretation and modeling,
993 Mathematical Geology, 33, 507-534, 2001.
994 Hoek, E. and Martin, C. D.: Fracture initiation and propagation in intact rock - A review,
995 Journal of Rock Mechanics and Geotechnical Engineering, 6, 14, 2014.
996 Huang, N., Jiang, Y., Liu, R., and Li, B.: Estimation of permeability of 3-D discrete fracture
997 networks: An alternative possibility based on trace map analysis, Engineering Geology, 226,
998 12-19, 2017.
999 Journel, A. and Zhang, T.: The Necessity of a Multiple-Point Prior Model, Mathematical
1000 Geology, 38, 591-610, 2006.
1001 Journel, A. G.: Beyond Covariance: The Advent of Multiple-Point Geostatistics. In:
1002 Geostatistics Banff 2004, Leuangthong, O. and Deutsch, C. V. (Eds.), Springer Netherlands,
1003 Dordrecht, 2005.
1004 Jung, A., Fenwick, D. H., and Caers, J.: Training image-based scenario modeling of fractured
1005 reservoirs for flow uncertainty quantification, Computational Geosciences, 17, 1015-1031,
1006 2013.
1007 Karimpouli, S., Tahmasebi, P., Ramandi, H. L., Mostaghimi, P., and Saadatfar, M.: Stochastic
1008 modeling of coal fracture network by direct use of micro-computed tomography images,
1009 International Journal of Coal Geology, 179, 153-163, 2017.
1010 Kovesi, P.: MATLAB and Octave Functions for Computer Vision and Image Processing. 2000.
1011 Lamarche, J., Chabani, A., and Gauthier, B. D. M.: Dimensional threshold for fracture linkage
1012 and hooking, Journal of Structural Geology, doi: https://doi.org/10.1016/j.jsg.2017.11.016,
1013 2017. 2017.

Lamarche, J., Lavenu, A. P. C., Gauthier, B. D. M., Guglielmi, Y., and Jayet, O.: Relationships between fracture patterns, geodynamics and mechanical stratigraphy in Carbonates (South-East Basin, France), Tectonophysics, 581, 231–245, 2012.

Laubach, S. E., Lamarche, J., Gauthier, B. D. M., Dunne, W. M., and Sanderson, D. J.: Spatial arrangement of faults and opening-mode fractures, Journal of Structural Geology, 108, 2-15, 2018.

Laubach, S. E., Olson, J. E., and Gross, M. R.: Mechanical and fracture stratigraphy, AAPG Bulletin, 93, 1413–1426, 2009.

Lavenu, A. P. C.: Relationships between fracture pattern and geodynamics in carbonates. Role of depositional facies, diagenesis and rock mechanical properties., Doctorate, CEREGE, Aix-Marseille Universite, 198 pp., 2013.

Lavenu, A. P. C., Lamarche, J., Gallois, A., and Gauthier, B. D. M.: Tectonic versus diagenetic origin of fractures in a naturally fractured carbonate reservoir analog (Nerthe anticline, southeastern France), AAPG Bulletin, 97, 2207-2232, 2013.

Liu, X., Srinivasan, S., and Wong, D.: Geological Characterization Of Naturally Fractured Reservoirs Using Multiple Point Geostatistics, 2002.

Liu, X., Zhang, C., Liu, Q., and Birkholzer, J.: Multiple-point statistical prediction on fracture networks at Yucca Mountain, Environmental Geology, 57, 1361-1370, 2009.

Lloyd, S. P.: Least Squares Quantization in PCM, IEEE Transactions on Information Theory, 28, 9, 1982.

Magistroni, C., Meda, M., and Corrao, A.: Faults and fracture network prediction: stress/strain modelling from outcrop analysis to seismic characterisation, Abu Dhabi, UAE, 10-13 November 2014 2014.

Mariethoz, G.: Geological stochastic imaging for aquifer characterization, Doctorate, Faculté des Sciences, Université de Neuchâtel, 229 pp., 2009.

Mariethoz, G., Renard, P., and Straubhaar, J.: The Direct Sampling method to perform multiplepoint geostatistical simulations., Water Resources research, 46, 2010.

Matonti, C., Lamarche, J., Guglielmi, Y., and Marié, L.: Structural and petrophysical characterization of mixed conduit/seal fault zones in carbonates: Example from the Castellas fault (SE France), Journal of Structural Geology, 39, 103-121, 2012.

Mauldon, M., Dunne, W. M., and Rohrbaugh, M. B. J.: Circular scanlines and circular windows: new tools for characterizing the geometry of fracture traces. , Journal of Structural Geology, 23, 12, 2001.

Meerschman, E., Pirot, G., Mariethoz, G., Straubhaar, J., Van Meirvenne, M., and Renard, P.: A practical guide to performing multiple-point statistical simulations with the Direct Sampling algorithm, Computers & Geosciences, 52, 307-324, 2013.

Micarelli, L., Benedicto, A., and Wibberley, C. A. J.: Structural evolution and permeability of normal fault zones in highly porous carbonate rocks, Journal of Structural Geology, 28, 1214-1227, 2006.

Montanari, D., Minissale, A., Doveri, M., Gola, G., Trumpy, E., Santilano, A., and Manzella, A.: Geothermal resources within carbonate reservoirs in western Sicily (Italy): A review, Earth-Science Reviews, 169, 180-201, 2017.

Olsson, R. and Barton, N.: An improved model for hydromechanical coupling during shearing of rock joints, International Journal of Rock Mechanics and Mining Sciences, 38, 13, 2001.

Otsu, N.: A Threshold Selection Method from Gray-Level Histograms, IEEE Transactions on Systems, Man, and Cybernetics, 9, 5, 1979.

Panza, E., Sessa, E., Agosta, F., and Giorgioni, M.: Discrete Fracture Network modelling of a hydrocarbon-bearing, oblique-slip fault zone: Inferences on fault-controlled fluid storage and migration properties of carbonate fault damage zones, Marine and Petroleum Geology, 89, Part 2, 263-279, 2018.

Reis, Á. F. C., Bezerra, F. H. R., Ferreira, J. M., do Nascimento, A. F., and Lima, C. C.: Stress magnitude and orientation in the Potiguar Basin, Brazil: Implications on faulting style and reactivation, Journal of Geophysical Research: Solid Earth, 118, 5550-5563, 2013.

Rogers, S. F.: Critical stress-related permeability in fractured rocks, Geological Society, London, Special Publications 2009, 10, 2003.

Rzonca, B.: Carbonate aquifers with hydraulically non-active matrix: A case study from Poland, Journal of Hydrology, 355, 202-213, 2008.

Somasundaram, S., Mund, B., Soni, R., and Sharda, R.: Seismic attribute analysis for fracture detection and porosity prediction: A case study from tight volcanic reservoirs, Barmer Basin, India, The Leading Edge, 36, 7, 2017.

Strebelle, S.: Conditional Simulation of Complex Geological Structures Using Multiple-Point Statistics, Mathematical Geology, 34, 1-21, 2002.

Suppe, J.: Geometry and kinematics of fault-bend folding, American Journal of Science, 283, 73, 1983.

Suppe, J.: Principles of structural geology, Prentice-Hall, Inc., Englewood Cliffs, New Jersey, 1985.

Tavani, S., Corradetti, A., and Billi, A.: High precision analysis of an embryonic extensional fault-related fold using 3D orthorectified virtual outcrops: The viewpoint importance in structural geology, Journal of Structural Geology, 86, 200-210, 2016.

Tavani, S., Storti, F., Lacombe, O., Corradetti, A., Muñoz, J. A., and Mazzoli, S.: A review of deformation pattern templates in foreland basin systems and fold-and-thrust belts: Implications for the state of stress in the frontal regions of thrust wedges, Earth-Science Reviews, 141, 82-104, 2015.

Van Eijk, M.: Analysis of the fracture network in carbonate rocks of the Jandaira Formation in northeast Brazil, 2014. Technische Universiteit Delft, 60 pp., 2014.

Vollgger, S. A. and Cruden, A. R.: Mapping folds and fractures in basement and cover rocks using UAV photogrammetry, Cape Liptrap and Cape Paterson, Victoria, Australia, Journal of Structural Geology, 85, 168-187, 2016.

Wang, S., Huang, Z., Wu, Y.-S., Winterfeld, P. H., and Zerpa, L. E.: A semi-analytical correlation of thermal-hydraulic-mechanical behavior of fractures and its application to modeling reservoir scale cold water injection problems in enhanced geothermal reservoirs, Geothermics, 64, 81-95, 2016.

Watkins, H., Healy, D., Bond, C. E., and Butler, R. W. H.: Implications of heterogeneous fracture distribution on reservoir quality; an analogue from the Torridon Group sandstone, Moine Thrust Belt, NW Scotland, Journal of Structural Geology, doi: https://doi.org/10.1016/j.jsg.2017.06.002, 2017. 2017.

Wu, J., Boucher, A., and Zhang, T.: A SGeMS code for pattern simulation of continuous and categorical variables: FILTERSIM, Computers & Geosciences, 34, 1863-1876, 2008.

Zhang, L., Kang, Q., Chen, L., Yao, J.: Simulation of flow in multi-scale porous media using the lattice boltzmann method on quadtree grids, Communications in Computational Physics 19, 17, 2016.